Vitamin D constrains inflammation by modulating the expression of key genes on Chr17q12-21.1

Ayşe Kılıç[1*], Arda Halu[1], Margherita De Marzio[1,2], Enrico Maiorino[1], Melody G. Duvall[3], Thayse Brueggemann[3], Joselyn J. Rojas Quintero[3], Robert Chase[1], Hooman Mirzakhani[1], Ayse Özge Sungur[4, 5], Janine Koepke[5], Taiji Nakano[6], Hong Yong Peh[3], Nandini Krishnamoorthy[3], Raja-Elie Abdulnour[3], Katia Georgopoulos[7], Augusto A. Litonjua[8], Marie B. Demay[9], Harald Renz[10, 11], Bruce D. Levy[3] and Scott. T Weiss[1*]

Affiliations:

1. Channing Division of Network Medicine, Department of Medicine, Brigham and Women's Hospital and Harvard Medical School, Boston MA, USA
2. Department of Environmental Health, Harvard TH Chan School of Public Health, Boston, MA, USA
3. Division of Pulmonary and Critical Care Medicine, Department of Medicine, Brigham and Women's Hospital and Harvard Medical School, Boston, MA, USA.
4. Behavioral Neuroscience, Experimental and Biological Psychology, Philipps-University Marburg, Marburg, Germany
5. Excellence Cluster Cardio-Pulmonary System (ECCPS), Justus Liebig University Giessen, Giessen, Germany
6. Department of Pediatrics, Graduate School of Medicine, Chiba University, Chiba, Japan
7. Cutaneous Biology Research Center, Massachusetts General Hospital, Harvard Medical School, Charlestown, Massachusetts, USA

8. Division of Pediatric Pulmonary Medicine, Golisano Children's Hospital at Strong, University of Rochester Medical Center, Rochester, NY, USA
9. Endocrine Unit, Massachusetts General Hospital and Harvard Medical School, Boston, MA, USA
10. Institute of Laboratory Medicine and Pathobiochemistry, Molecular Diagnostics, Philipps University of Marburg, Marburg, Germany; German Center for Lung Research (DZL).
11. Department of Clinical Immunology and Allergology, Laboratory of Immunopathology, Sechenov University, Moscow, Russia

*Correspondence should be addressed to A.K. (ayskilic@gmail.com) or S.T.W (scott.weiss@channing.harvard.edu).

Keywords: Vitamin D, airway inflammation, Th2 cells, Chr17q12-21, autoimmunity, immunomodulation, AIOLOS

Summary

Vitamin D possesses immunomodulatory functions and vitamin D deficiency has been associated with the rise in chronic inflammatory diseases, including asthma [1]. Vitamin D supplementation studies do not provide insight into the molecular genetic mechanisms of vitamin D mediated immunoregulation. Here we provide evidence for vitamin D regulation of two human chromosomal loci, Chr17q12-21.1 and Chr17q21.2, reliably associated with autoimmune and chronic inflammatory diseases [2–4]. We demonstrate increased vitamin D receptor (VDR) expression in mouse lung CD4+ Th2 cells, differential expression of Chr17q12-21.1 and Chr17q21.2 genes in Th2 cells based on vitamin D status and identify the IL-2/Stat5 pathway as a target of vitamin D signaling. Vitamin D deficiency caused

severe lung inflammation after allergen challenge in mice that was prevented by long term prenatal vitamin D supplementation. Mechanistically, vitamin D induced the expression of the *Ikzf3* encoded protein Aiolos to suppress IL-2- signaling and ameliorate cytokine production in Th2 cells. These translational findings demonstrate mechanisms for the immune protective effect of vitamin D in allergic lung inflammation with a strong molecular genetic link to the regulation of both Chr17q12-21.1 and Chr17q21.2 genes and suggest further functional studies and interventional strategies for long- term prevention of asthma and other autoimmune disorders.

Results

To address the genetic and molecular mechanisms by which vitamin D can influence asthma, allergic and autoimmune disease risk, we studied the genetic loci of two chromosome regions of interest: 1) the 17q12-21.1 region, that includes the well-known asthma-associated *ORMDL3* gene [5], and 2) the 17q21.2 region, that includes the *STAT5* gene, known to be extensively associated with autoimmune diseases [6,7]. We first examined the entire set of significant disease and trait associations in the Chr17q12-21.1 (181 associations) and Chr17q21.2 (100 associations) loci using the NHGRI-EBI GWAS Catalog [8]. Both regions had multiple Th1 and Th2 diseases associations with at least one significant SNP. Chr17q12-21.1 had the highest number of associations related to Th2 diseases (Fig. 1a) and 17q21.2 had the highest number of associations related to Th1 diseases (Extended Data Fig. 1a). To address the possible link to vitamin D intake, we next investigated a potential overlap of these SNPs with VDR binding sites. Out of the 169 VDR binding sites on Chr17, seven were located in the 17q12-21.1 locus, concentrated in two bands on or near *IKZF3* and *ZPBP2* (Fig. 1b). These VDR binding sites also overlapped with RXRA binding sites (Fig. 1b). To assess their functional relevance, we searched for eQTLs in these VDR binding regions. We found that four cis-eQTLs control *IKZF3* expression in whole blood and EBV-transformed lymphocytes: rs2941522 and rs12946510 in the enhancer region targeting *ORMDL3* and *IKZF3*, and rs1453559 and rs35564481 in the enhancer region targeting *ORMDL3*, *GSDMA* and *GSDMB* (Fig. 1b). Rs1453559 and rs2941522 have previous GWAS associations with

both asthma and autoimmune diseases[9–11], rs12946510 has previous GWAS associations with autoimmune diseases[12,13], and rs35564481 has no known GWAS associations. For the 17q21.2 locus, the only VDR binding site resides near the gene *PSMC3IP* in an enhancer site targeting *STAT5A* (Extended Data. Fig. 1b). PSMC3IP expression is controlled by three eQTLs overlapping with this VDR binding site (rs4793244, rs62078362 and rs111708606), none of which have any known disease associations. These results suggest that vitamin D binding is critical in this genomic region.

We next examined the linkage disequilibrium (LD) pattern between the Th1/Th2-associated SNPs and the SNPs in the VDR binding sites (Fig. 1c). Out of the seven SNPs with VDR binding sites identified in 17q12-21.1 and 17q21.2, the first four in 17q12-21.1 (rs2941522, rs12946510, rs35564481, rs1453559) were in a high-LD block with many other Th1-Th2 associated SNPs in the same region. These same four SNPs in 17q12-21.1 were also in high-LD with two SNPs in *ZPBP2* and *ORMDL3* (rs12936231 and rs4065275, respectively) that were previously shown to be functionally relevant to asthma [3,4,14]. Additionally, two of the three SNPs with VDR binding sites in 17q21.2 (rs4793244 and rs62078362) were in strong-LD with three other Th1-Th2 associated SNPs in the17q21.2 region (rs11871801, rs2006141, rs4793090). Overall, these results highlight strong statistical association between vitamin D binding sites and multiple genotypic variations linked to asthma, autoimmune and allergic diseases.

Two SNPs in *ZPBP2* and *ORMDL3* (rs12936231 and rs4065275, respectively) that were previously shown to be functionally relevant to asthma [3,4,14], were also in high linkage disequilibrium with the four SNPs that we identified in the VDR binding regions of the 17q12-21.1 loci (Fig. 1c). Importantly, in both the 17q12-21.1 and 17q21.2 regions, the VDR binding sites coincide with CTCF and IKZF3 binding sites, as well as H3K27ac peaks indicating active enhancer sites (Fig. 1b and Extended Data Fig. 1b). In particular, the two enhancer sites in 17q12-21.1 (GH17J039753 and GH17J039859) were both predicted to interact with the *ORMDL3* promoter region (Fig. 1b), and the enhancer site in 17q21.2 (GH17J042576) was predicted to interact with the *STAT5A* promoter region (Extended

Data Fig. 1b). This suggests a similar mechanism to the one described in [4], whereby SNPs in LD with each other in these enhancer sites affect VDR and CTCF binding, the co-dependence of which in turn could modulate *ORMDL3* and *STAT5A* expression. Although it has been shown that CTCF binding sites can be vitamin D-sensitive[15], no such sites were found in our genomic regions of interest (Fig. 1b and Supp. Fig. 1b).

Next, we investigated cord blood gene expression data in the Vitamin D Antenatal Asthma Reduction Trial (VDAART) (see Methods) and looked at the genes of interest in the 17q12 and 17q21 regions and their interaction with cord blood vitamin D levels as predictors of asthma/wheeze risk at age 3 year of age. After adjusting for relevant covariates (see Methods), the baseline expression term of *IKZF3* was not found to be significantly associated with asthma risk, while the interaction between vitamin D and *IKZF3* was statistically significant (p-val. < 0.05), suggesting that the association of *IKZF3* expression with asthma risk was mediated by vitamin D levels in the cord blood (Extended Data Table 1).

Based on our bioinformatic analysis of the Chr17q12 and 17q21 regions, we hypothesize that low vitamin D tissue levels is associated with decreased *IKFZ3* expression and increased expression of *ORMDL3*, *STAT3*, *STAT5A*, *STAT5B*, and *IL2*.

Vitamin-D receptor (VDR) is expressed in Th2 cells in allergic airway inflammation

To test our hypothesis of vitamin D activity at the Chr17q12-21 locus we utilized a mouse model of allergic airway inflammation and identified vitamin D responsive leukocyte subsets in house dust mite (HDM)-sensitized and challenged mice using flow cytometry (Fig.2a, Extended Data Fig. 2a-c). VDR expression was significantly induced in HDM sensitized and challenged mice and almost absent in leukocytes isolated from control (vehicle) lungs (Extended Data Fig. 2c) but. Within the CD45+ population, VDR expression was high in CD4+ T cells (p= 0.0357), while only very few CD8+ T cells and CD19+ B cells expressed VDR (Fig. 2b, Extended Data Fig. 2c HDM). Within the CD4+ T cell population, highest VDR expression was detected in Gata3+ Th2 cells (p= 0.002 vs Tbet+ and p< 0.0001 vs Foxp3+ T cells). VDR expression was very low in Tbet+ Th1

and CD4+ Foxp3+ Treg cells (Fig. 2b). The differential expression of VDR in Th2 cells was further validated by western blot analysis using naïve CD4+ T cells immediately after isolation (0hrs), after activation with CD3/CD28 for 48 hrs and in *in vitro* polarized Th1, Th2 and iTreg cells with well-defined culture conditions (Extended Data Fig. 3a, see Methods section). VDR expression appeared as early as day 1 of Th2 culture conditions and gradually increased during the polarization process (Extended Data Fig. 3b). In the absence of the VDR ligand vitamin D, VDR expression localized to the cytoplasm of Th2 cells. Addition of the VDR ligand calcitriol led to a strong translocation of VDR into the nucleus, suggesting functionality of the expressed receptor in the presence of its ligand (Extended Data Fig. 3c). These results identify Th2 cells as vitamin D targets in allergic airway inflammation.

Vitamin D status regulates the expression of key genes on Chromosome17q12-21.1 and Chr17q21.2

Taking cell type specific gene expression and selective expression of VDR in Th2 cells into account, we next analyzed the expression of genes encoded on Chr17q12-21.1 and 17q21.2 loci in WT and vitamin D deficient Th2 cultures as well as in Th2 cells post calcitriol stimulation.

Vitamin D deficiency differentially regulated the expression levels of several Chr17q12-21.1 encoded genes, with lower expression of *Ikzf3*, *Ormdl3* and *Gsdma* (all p=0.0286) (Fig. 2d). Conversely, stimulation with calcitriol induced the expression of the same genes (all p=0.043) (Fig. 2e). Expression of the Chr17q21.2 genes *Stat3*, *Stat5a* and *Stat5b* was not affected by vitamin D deficiency (Fig.2f). However, after calcitriol stimulation *Stat5a* (p=0.0082) and *Stat5b* (p=0.003) genes were strongly suppressed and *Stat3* (p= 0.0048) expression was increased in Th2 cells. (Fig. 2g). These results hint to a protective role of vitamin D in allergic airway inflammation, by regulating the expression of the IL-2 downstream signaling molecules *Stat5a* and *Stat5b*.

Deficiency in vitamin D signaling augments allergic airway inflammation

To decipher the protective role of vitamin D signaling in allergic airway inflammation, we employed vitamin D deficient and $VDR^{-/-}$ mice (Fig. 3a) [16]. HDM sensitization of vitamin D

deficient mice led to a stronger reaction to the allergen resulting in more prominent peri-bronchial and perivascular leukocytic infiltrates (Fig. 3b). This phenotype was accompanied by lower VDR expression in CD4+ T cells isolated from HDM-exposed lungs compared to WT (Fig. 3c). Vitamin D deficiency led to a robust increase in total immunoglobulin (Ig)E levels (Fig. 3d). Histological findings were associated with higher total BAL leukocyte ($p= 0.0008$) (Fig. 3e), eosinophil ($p= 0.0002$) (Fig. 3f) and lymphocyte ($p= 0.0023$) (Fig. 3g) numbers in vitamin D deficient mice. Th2 cell numbers ($p= 0.0127$) were also higher in the HDM exposed mice (Fig. 3h) in a manner that was independent of T helper cell skewing (Extended Data Fig. 4a, b). Differentiation and recruitment of Th17 and IL-10 producing CD4+ T cells was not affected by vitamin D deficiency (Extended Data Fig. 4a, b). To validate these findings from vitamin D deficiency, we next employed $VDR^{-/-}$ mice (see Methods). As with the vitamin D deficient mice, HDM sensitization and challenge of $VDR^{-/-}$ mice led to an increased Th2 immune response. The lung phenotype in the $VDR^{-/-}$ mice was marked by dense leukocytic infiltrates around and mucus plugs in the airways (Fig. 3b). The augmented systemic and local immune response increased total IgE titers ($p= 0.0489$), and total BAL ($p< 0.0001$ vs WT HDM and $p= 0.003$ vs Vit D deficient HDM), eosinophil ($p< 0.0001$ vs WT HDM and Vit D deficient HDM), total lymphocytes ($p=0.0194$ vs WT HDM and $p= 0.0421$vs Vit D deficient HDM) and Th2 cells ($p= 0.0009$ vs WT HDM) (Fig. 3. d-h). $VDR^{-/-}$ did not significantly affect recruitment of Treg and Th17 cells (Extended Data Fig. 4a, b).

To explore the mechanisms underlying the augmented Th2-phenotype in the lungs of vitamin D deficient and $VDR^{-/-}$ mice after HDM allergen challenge, we analyzed the transcriptional profiles of in vitro polarized Th2 cells from WT and vitamin D deficient mice (Fig.3i). Differential expression and enrichment analysis revealed dysregulation of several pathways implicated in Th2-cell activation, cytokine production, proliferation, and survival with prominent changes in the IL-2/ STAT5 - pathway in vitamin D deficient Th2 cells ($p= 0.0014$) (Fig. 3j, Extended Data Table 2 & 3). The effects of impaired vitamin D signaling on these pathways was confirmed by qRT-PCR and flow cytometry. Baseline expression of IL-2 was markedly increased at both the RNA ($p= 0.0286$)) and protein levels ($p= 0.0079$) in vitamin D deficient and $VDR^{-/-}$ Th2 cells (Fig. 3k, l). In Vitamin D deficient and

VDR$^{-/-}$ Th2 cell *in vitro* incubation, the elevated IL-2 levels were accompanied by a sharp increase in IL-13 production (VitD deficient: $p < 0.0001$; VDR$^{-/-}$: $p = 0.0141$) (Extended Data Fig. 5).

Taken together, these results indicate a critical role for vitamin D/VDR signaling in regulating type 2 inflammation and identify the IL-2/ Stat5 pathway as a downstream target of vitamin D in Th2 cells.

Vitamin D suppresses the activation of the IL-2/Stat5 pathway and cytokine production in Th2 cells

To ascertain the vitamin D dependent regulation of the IL-2/Stat5 pathway and the impact on the effector program of Th2 cells, we first analyzed the transcriptional profile of WT Th2 cells exposed to calcitriol during differentiation (Fig. 4a). Gene ontology enrichment analysis of biological processes revealed regulation of several processes impacting inflammatory responses, including chemotaxis and activation of cells (Extended Data Table 4). Calcitriol stimulation of Th2 cells affected several immune related disease pathways, including asthma (Extended Data Fig. 6, Extended Data Table 5). Gene set enrichment analysis (GSEA), performed on the differentially expressed genes, highlighted the negative regulation of IL-2/Stat5 pathway in Th2 cells by calcitriol (Fig. 4b, Extended Data Table 6). Calcitriol stimulation suppressed the expression of *Il2* ($p<0.0001$), *Stat5a* ($p<0.0008$) and *Stat5b* ($p<0.0008$) genes (Fig. 4c). Concordantly, levels of activated Itk (phospho-Itk) ($p = 0.029$) and expression of the IL2Rβ (CD25) ($p = 0.0441$) were reduced on a per cell basis (Fig. 4d).

Next, the impact of calcitriol stimulation on the effector function of Th2 cells was assessed by flow cytometric analysis for the T2 cytokine IL-13. Activation of the vitamin D/VDR pathway led to significant suppression of IL-13 production in CD4+ T cells ($p = 0.0012$) (Fig. 4e).

To further delineate the molecular impact of vitamin D on Th2 cell biology, we integrated the murine transcriptional profile with a recently developed human Protein-Protein

Interaction (PPI) database[17] . By modeling the signal transduction process as a sequential path on the PPI network that starts from a receptor and propagates downstream to a transcription factor via multiple intermediate proteins (for details see Methods section, Extended Data Fig. 7a), we inferred the active signaling flow in Th2 cells for control (vehicle) and calcitriol stimulated Th2 cells. As input of our network analysis, we selected a subset of receptors and transcription factors that are known to be involved in CD4+ T cell activation, Th2 cell differentiation, and cytokine production (Extended Data Table 7). For clarity of the figure, we display the gene names. Corresponding protein names are attached in Extended Data Table 8. In control Th2 cells, our network analysis revealed the engagement of a variety of receptors including IL4R, IL2RA, CD28, and TNF-receptors. Downstream to these receptors, the most active signaling paths highlighted the activation of STAT3, STAT5A/B, NFkB1, and IKZF1 transcription factors (Extended Data Fig. 7b) via multiple adapter proteins of the TRAF and JAK family. Interestingly, these transcription factors are known to be involved in differentiation and activation pathways in Th2 cells Conversely, after calcitriol stimulation, signal from IL4R, CD28 and TNFSF8 propagated over different interaction partners (Fig. 4f). Calcitriol specific edges are highlighted in orange color. Molecular mediators included the cytoskeletal proteins VAV1 and RACK1 and emphasized activation of the transcription factors AP-1 (FOS/JUND dimer) and NFATC1.

Our network analysis highlighted a central role of the transcriptional repressor IKZF1 (IKAROS) upon calcitriol stimulation, which was targeted by multiple downstream mediators including IKZF3 (AIOLOS). Notably, the IKZF3 gene encodes for the AIOLOS protein, a direct interaction partner of the IKZF1-encoded IKAROS. Both transcription factors, as homo- and heterodimers, suppress IL-2 expression on the transcriptional levels in mouse and human lymphocytes[18]. Calcitriol increased the number of edges connecting intermediate proteins to the transcriptional repressor IKAROS. Among the connecting proteins, AIOLOS interaction with IKAROS was implicated in repression of IL-2 expression in Th2 cells by vitamin D. Absence of STAT5A/B mediators in the active signaling paths of calcitriol stimulated Th2 cells further suggested repression of the Th2 cell STAT5 pathway with calcitriol compared to control (Extended Data Fig. 7b).

Taken together, these results indicate that the specific suppression of the IL-2/Stat5 pathway by vitamin D results in reduced cytokine production by Th2 cells. Our findings suggest that this suppression was mediated by the vitamin D dependent regulation of IKAROS (IKZF1) through the induction of AIOLOS (IKZF3).

Vitamin D supplementation alleviates the allergic phenotype in the lung by suppressing type 2 cytokine production in a dose dependent manner

To test if vitamin D supplementation prevents the development of T2 driven allergic inflammation in the lung, custom rodent diets with select vitamin D doses were used: 400 IU/kg chow (400 IU; low), 1000 IU/kg chow (1000 IU; regular) and 4000 IU/kg chow (4000 IU; high) (see Methods section). The 1000 IU group was used as the control group, as it contains the average amount of vitamin D fortified in standard rodent chow. HDM exposure led to recruitment of leukocytes into the lung tissue and BAL (Fig. 5a, b), with a predominant eosinophilic and lymphocytic infiltrate as well as high numbers of IL-13+ Th2 cells (Fig. 5c-e). There were trends for higher cellular infiltration in the airways when mice were supplemented with the low vitamin D doses (400 IU), but these inflammatory responses were not significantly different from the phenotype observed with 1000 IU. Lung and airway pathology were similar between these dosing groups, with similar numbers and frequencies of the different leukocyte populations. In sharp contrast, dietary supplementation with the higher vitamin D dose (4000 IU) decreased the inflammatory phenotype in HDM exposed mice compared to the 400 IU and 1000 IU dosed animals. Concordant with the histological findings, BAL leukocytes ($p< 0.0001$) were decreased with marked reductions in BAL eosinophil ($p=0.0016$) and lymphocyte numbers ($p=0.026$) (Fig. 5c-d), and the frequency of IL-13+ Th2 cells was significantly reduced in the lungs with 4000 IU of vitamin D ($p= 0.0066$ vs 400 IU HDM; $p=0.0011$ vs 1000 IU HDM) (Fig. 5e). Of note, dietary supplementation with high vitamin D levels, increased VDR expression in CD4+ T cells from HDM exposed lungs ($p< 0.0001$) (Extended Data Fig. 8b).

To ascertain that dietary supplementation with vitamin D specifically altered mouse Th2 cell differentiation and the effector program, splenic naïve CD4+ T cells from 400 IU and

4000 IU mice were studied. Of interest, naïve CD4+ T cells did not express VDR until they were exposed to Th2 polarizing conditions. Gata3 expression on per cell basis was lower in 4000 IU Th2 cells (p= 0.0286) (Extended Data Fig. 9a). This was accompanied by higher VDR protein expression (p= 0.0286) (Extended Data Fig. 9b). The expression of IL-2 (p= 0.0004) and the Th2 cytokines IL-13 (p= 0.0159) and IL-5 (p= 0.0159) were lower in 4000 IU Th2 cultures (Extended Data Fig. 9c-f).

To explore the specific induction of Aiolos expression for vitamin D mediated suppression of IL-2 production in Th2 cells, Aiolos expression was monitored throughout Th2 differentiation. Aiolos expression gradually increased under Th2 polarizing conditions in CD4+ T cells, starting as early as day 1 of in vitro culture (Fig. 5f). Simultaneous exposure to calcitriol further increased Aiolos protein levels compared to vehicle in Th2 cells (p= 0.0079) (Fig. 5g).

To test if vitamin D exerts its inhibitory effect on IL-2 production via Aiolos induction, Ikzf3$^{-/-}$ mice were employed, exposed to Th2 polarizing conditions and assessed for IL-2 production after calcitriol exposure. IL-2 production in control Ikzf3$^{-/-}$ Th2 cultures was significantly higher compared to WT Th2 cells. Calcitriol significantly reduced IL-2 levels in both, WT (p= 0.0001) and Ikzf3$^{-/-}$ Th2 cells (p= 0.0001) (Fig. 5h); however, the suppressive effect of calcitriol on IL-2 production was significantly higher in WT Th2 cells (~ 65% inhibition) compared to Ikzf3$^{-/-}$ Th2 cells (~40% inhibition) (p= 0.0001) (Fig. 5h).

Taken together, these results indicated that vitamin D can regulate Aiolos expression and suggested a role for Aiolos as a downstream effector for selectively fine-tuning Th2 cell IL-2 production by vitamin D.

Discussion

We utilized human genetics to identify SNPs on chromosome 17q12-21.1 and 17q21.2 that were within GWAS regions for Th1 and Th2 autoimmune diseases. Of note, many of these SNPs were within VDR binding sites. We then determined by eQTL analysis of the genes in these two genomic regions that IKZF3 expression was controlled by four cis-

eQTLs in the enhancer region targeting ORMDL3 and IKZF3, and in the enhancer region targeting ORMDL3, GSDMA and GSDMB. Next, we demonstrated that two SNPs in CTCF binding sites were in strong LD with these 4 eQTL SNPs and that the two enhancer sites in 17q12-21.1 were both predicted to interact with the ORMDL3 promoter region, and the enhancer site in 17q21.2 was predicted to interact with the STAT5A promoter region thus, suggesting a plausible human molecular genetic mechanism by which vitamin D could activate IKZF3 to repress ORMDL3 and immune system development. Finally, we leveraged bulk RNAseq in the cord blood of the VDAART trial to show that an interaction for vitamin D level and IKZF3 expression that was associated with reduced asthma risk at 3 years of age.

The vitamin D receptor was genetically associated with asthma in 2004[19] and high intake of vitamin D by pregnant women is associated with about a 50% reduction in asthma risk in the mother's offspring[15,20]. Together, these exciting findings led to a comprehensive theory about how vitamin D deficiency could influence asthma occurrence through its effects on lung and immune system development and that progressive decreases in vitamin D intake from 1946 onward could be contributing to the epidemic of allergic and autoimmune diseases[1]. Vitamin D deficiency is the most common vitamin deficiency in the world today and is particularly prevalent in pregnant women where the fetal lung and immune system are developing[21–23].

To determine the impact of vitamin D supplementation, we performed a clinical trial, the Vitamin D Antenatal Asthma Trial (VDAART) in pregnant women who either had allergies or asthma or had family members with these conditions. The participants were given either 4400 IU of vitamin D3 or 400 IU and were followed throughout their pregnancy and for the first six years of the life of the child[24]. The results of the trial were not statistically significant using conventional intent to treat analysis[25,26] but the reasons were complex, as is often seen when the effects of nutrients are studied. Most importantly, unlike conventional drug trials where one compares drug to no drug or alternative drug, in nutrient trials there is nutrient already present in the placebo group. This creates misclassification that can reduce trial power. When we performed a meta-analysis of the

two pregnancy related trials of vitamin D, we got a statistically significant reduction in asthma in the offspring of women who had the higher vitamin D intake during pregnancy and, when we adjusted for the baseline level of vitamin D in the meta-analysis, we got a reduction in asthma risk of 50 percent, exactly what we saw in the observational studies performed previously[27,28].

To link the results of the VDAART trial directly to the chr17q12 locus we genotyped SNP, rs12936231, in ZPBP2, the gene adjacent to ORMDL3, and stratified the VDAART trial results by maternal genotype at this locus and found that the vitamin D effect in the trial was significantly influenced by genotype with the GG genotype exhibiting a protective effect on asthma risk in the child and the CC or GC genotype not being responsive to vitamin D, additionally this result was related to sphingolipid production with the children protected from asthma having higher sphingolipid production[3].

This SNP (rs12936231) is one of two SNPs (the other being rs4065275) that alter the chromatin state of a regulatory domain, specifically two CTCF binding sites, in the chr17q12-21.1 locus that are correlated with the expression of ORMDL3[4,14]. 4C-seq assays previously demonstrated that the ORMDL3 promoter interacts with a long-range enhancer in IKZF3 that promotes (or represses) transcription of ORMDL3 in cells expressing both genes and the binding of CTCF per the G allele of rs12936231 in ZPBP2 blocks this interaction resulting in reduced transcription of ORMDL3 on haplotypes with the rs12936231-G allele[4]. If rs12936231 is not activated then there is activation of the other CTCF binding site (rs4065275) intronic to ORMDL3 thus favoring the expression of ORMDL3 and increased asthma risk[4].

Mouse models have contributed to our understanding of ORMDL3 function as mice expressing the ORMDL3 transgene exhibit spontaneous increases in airway hyper responsiveness, the essential feature of asthma. This increase in AHR was associated with airway remodeling and peri bronchial fibrosis without airway inflammation[29]. ORMDL3 is pleotropic, influencing Ca++ signaling, and the unfolded protein response. Most importantly, increased expression of ORMDL3 inhibits the

enzyme serine palmityl-transferase, the rate limiting step in the production of sphingolipids and ORMDL3 TG mice have reduced levels of sphingolipids[30]. What has been unclear is how ORMDL3 is controlled.

To confirm our human molecular genetic findings, we chose to utilize mouse models of allergic lung inflammation. We show strong VDR expression in CD4+ Th2 cells and alterations in chr17q12-21.1 and 17q21.2 gene expression induced by vitamin D status. Expression of VDR has been reported for airway epithelial cells and different immune cell types present in the lung[31]. In lymphocytes, *ex vivo* and *in vitro* studies describe low baseline VDR transcript expression levels that were transiently increased by activating signals and calcitriol stimulation[32]. Here, we report a differential VDR expression pattern in CD4+ T cell subsets in allergic inflamed lungs and post lineage specific cytokine stimulation *in vitro*, with strongest expression in Th2 cells. Activation of VDR suppressed IL-2, IL-5, and IL-13 production by Th2 cells. The expression of VDR in Gata3+Th2 cells in the lung might represent an endogenous control mechanism to curb the pathogenic cell activity and cytokine production after repetitive allergen contact. *Ex vivo* and *in vitro* Th1, nTreg and iTreg cells expressed low VDR protein levels at baseline. It remains to be determined whether other Th-subsets described in allergic inflammation express VDR at baseline and if either calcitriol or other secondary signals, specific for each subset, could induce VDR expression during inflammation.

Vitamin D deficiency that had been introduced over two generations and impaired vitamin D signaling led to an augmented allergic phenotype in the lung after allergen exposure with a dominating Th2-signature locally and systemically. This had likely been due to specific deregulation of Th2 cells instead of Th cell skewing, since neither Th17 nor Treg development and recruitment had been significantly affected. In contrast, in mice supplemented with high vitamin D doses over two generations, VDR expression and consequently vitamin D responsiveness was higher in CD4+ T cells from the animals' lungs, almost abrogating the inflammatory process in the lung after allergen challenge. While the vitamin D dose had been chosen to replicate the VDAART trial in the mouse, the duration of supplementation was adopted to the protocol of generating vitamin D

deficient mice. Both factors might influence the outcome here compared to prior rodent studies with inconclusive results.

Differentiation of Th2 cells is driven by IL-4 induced Gata3 expression in naïve CD4+ T cells. This process depends on a positive feedforward loop by IL-2 and its downstream STAT5 signaling pathway for the effective expression of IL-4[33]. Therefore, either interfering with Gata3 expression or the IL-2 pathway represents a promising strategy to finetune Th2-driven immunity. Our data highlight the specific regulation of the IL-2/STAT5 pathway by vitamin D. Vitamin D deficiency and impaired VDR signaling caused elevated IL-2 production by Th2 cells, mounting in high IL-13 production. Elevated IL-13 levels *in vivo*, could amplify the local T2 responses in the lung. In sharp contrast, exposure of polarizing Th2 cells to calcitriol was able to suppress IL-2 production, expression and activation of STAT5A/B and therefore IL-13 production by Th2 cells. The transcription factor AIOLOS has previously been shown to suppress IL-2 expression on the transcriptional level[18]. We report here a vitamin D mediated induction of Aiolos expression in Th2 cells, which is impaired by vitamin D deficiency. High Aiolos expression coincided with lower IL-2 production, ameliorated STAT5A/B expression, and IL-13 production in Th2 cells. *In vitro* Th2 polarization of naïve CD4+ T cells isolated from mice supplemented with higher vitamin D levels, without further exogenous calcitriol stimulation, developed a weakened Th2 phenotype, characterized by lower IL-2, IL-5, and IL-13 production. Since naïve CD4+ T cells do not express VDR, these results implicate changes in chromosomal accessibility by high vitamin D in the developing immune system, which needs further investigation.

Experiments here with Ikzf3$^{-/-}$ mice demonstrated significant reductions in vitamin D mediated control of Th2 cell cytokine production, but the vitamin D response was not completely impaired, suggesting additional mechanisms for vitamin D regulation of Th2 cells – several possibilities were uncovered by our PPI analyses. These will be the subject of future research. In addition, we only investigated a Th2 mouse model of asthma and have not extended our mouse work to Th1 models of autoimmunity. We have still to consider other genes that might be linked to these two genetic loci and there are likely

455 other VDR binding sites of importance in both asthma and Th1 autoimmunity. More work
456 to determine the exact levels of vitamin D that confer this protective effect would also be
457 worthy of further investigation.
458
459 In summary, we have leveraged clinical trial data, molecular genetic bioinformatic data
460 and mouse model data to outline for the first time, a comprehensive molecular genetic
461 mechanism for how vitamin D influences not only asthma, but both Th1 and Th2
462 autoimmune disease. The significance of these findings relates to the high prevalence of
463 vitamin D deficiency, especially during pregnancy, and the strong possibility that the
464 epidemic of asthma and autoimmunity might be significantly reduced if vitamin D levels
465 were elevated worldwide.
466
467
468 **Figure Legends**
469 **Figure 1. VDR binding sites on Chr17q12 and q21.1 overlap with open chromatin**
470 **signatures. a,** Significant disease, and trait associations in 17q12-21.1 (y-axis), retrieved
471 from the NHGRI-EBI GWAS Catalog, with at least one significant SNP (x-axis) in
472 Chr17q12-21.1. Colored bars denote autoimmune diseases mapped to Th1 (red bars) or
473 Th2 (blue bars) driven immunity. **b,** University of California Santa Cruz (UCSC) Genome
474 Browser tracks showing chromosomal location, common dbSNPs, VDR-, RXR-, CTCF-
475 and IKZF3-binding sites and H3K27Ac marks present in the Chr17q12-21.1 locus. VDR
476 binding sites overlapping with active regulatory elements are highlighted by colored
477 boxes. **c**, Linkage disequilibrium (LD) between the significant SNPs in the Chr17q12-21.1
478 (magenta) and 21.2 (green) region, highlighting Th1/Th2-associated SNPs (red and blue,
479 respectively), eQTLs in the VDR binding regions in Chr17q12-21.1 and 21.2 (yellow), and
480 functional asthma SNPs from the literature (cyan).
481
482 **Figure 2. VDR expression is elevated in Th2 cells and vitamin D regulated**
483 **expression of genes on Chr1q12 and Chr17q21. a,** Scheme of the house dust mite
484 (HDM) induced airway inflammation protocol. **b,** Flow cytometric analysis and cell
485 frequencies of VDR expression in CD45+ CD4+ T cells in the respective groups (n=4-5).

c, Flow cytometric analyses and cell frequencies of VDR expression in Th1 (Tbet+), Th2 (Gata3+) and Treg (Foxp3+) cells in the respective groups (n=4-7). Quantitative RT-PCR analysis of relative mRNA expression levels of genes encoded on Chr17q12-21.1 in Th2 cultures of WT and vitamin D deficient mice (**d**) and control and calcitriol stimulated cultures (**e**). Quantitative RT-PCR analysis of relative mRNA expression levels of genes encoded on Chr17q21.2 in Th2 cultures of WT and vitamin D deficient mice (**f**) and control and calcitriol stimulated cultures (**g**). Gene expression levels were normalized to the house keeping gene *L32* and are expressed relative to the expression level in WT (**d, f**) or WT-vehicle (**e, g**) Th2 cells. (n ≥ 4 per group). Each symbol represents one mouse. Numbers in flow plots indicate percentages. Error bars indicate the s.e.m. Statistical tests: two-tailed Mann-Whitney U test (**b, c**). *P < 0.05, **P < 0.01, ***P < 0.001. Data summarize results from two independent experiments.

Figure 3. Vitamin D deficiency augments allergic airway inflammation. a, Schematic presentation of the different mouse strains used. **b,** Representative H&E-stained lung sections from saline and HDM-exposed wild type (C57/BL6; WT), vitamin D deficient and $VDR^{-/-}$ mice (x 10 magnification). Black arrows point to the peri bronchial infiltrate. **c,** Representative flow plots assessing VDR expression in lung CD4+ T cells from the indicated groups. **d,** Total IgE levels detected in the sera of respective groups. **e- g,** Absolute numbers of leukocytes (**e**), eosinophils (**f**) and lymphocytes (**g**) in the airways of the respective groups. **h**, Frequencies of IL-13 producing Th2 in the lung. **i,** Heat map showing differentially expressed genes between WT and vitamin D deficient Th2 cultures identified by RNA-Sequencing analysis. Analysis and visualization were performed with DESeq2. **j**, Overrepresentation analysis of Hallmark gene sets in the differentially expression gene set. The x-axis represents the gene ratio in the respective gene set. Dot sizes denote the number of genes in the respective pathway. The dot color indicates the FDR-adjusted p-value. Analysis and visualization were performed with the clusterProfiler package. **k,** Quantitative RT-PCR analysis of *Il-2* mRNA expression in Th2 cultures from the respective groups (n=4 per group). Gene expression levels were normalized to the house keeping gene *L32* and are expressed as fold-induction compared to WT Th2 cells. **l**, Flow cytometric analysis and cell frequencies of IL-2 production in WT and $VDR^{-/-}$ Th2

cultures (n=5 per group). Each symbol represents one mouse. Error bars indicate the s.e.m. Statistical significance was determined with: Mixed-effect analysis with Holm-Šidák's post-hoc analysis (**d –h**), two-tailed Mann-Whitney U test (**k, l**). *P < 0.05, **P < 0.01, ***P < 0.001, ****P < 0.0001. Data summarize results from two or three independent experiments with n>8 per group.

Figure 4. Vitamin D stimulation of polarizing Th2 cells suppresses the IL-2/Stat5 pathway. a, Heat map of differentially expressed genes between vehicle (EtOH [% v/v]) and calcitriol treated WT Th2 cells. Analysis and visualization were performed with DESeq2. **b**, Gene set enrichment analysis (GSEA) of differentially expressed genes. Analysis and visualization were performed with the clusterProfiler package. **c**, Quantitative RT-PCR for *Il-2*, *Stat5a* and *Stat5b* mRNA expression in Th2 cells exposed to either vehicle or calcitriol. Gene expression levels were normalized to the house keeping gene *L32* and are expressed as fold-induction compared to control cells. **d**, Flow cytometric analysis and mean fluorescence intensities of Itk and Il2rβ expression in indicated groups. **e**, Flow cytometric analysis and quantification of IL-13 expression in respective groups. **f**, Network analysis to visualize vitamin D induced molecular changes in the molecular interactome of calcitriol stimulated CD4+ Th2. Predefined set of cell membrane receptors were set as starting points (orange nodes) and annotated transcription factors were set as ending points (blue). All intermediate proteins on the PPI are visualized as grey nodes. Molecular interactions only overrepresented in calcitriol stimulated cells are shown as orange arrows. Each symbol in the bar graphs represents one individual sample and data summarize the results from two or three independent experiments with n≥ 5. Error bars indicate the s.e.m. Statistical test: two-tailed Student's t-test (**c, e**) and two-tailed Mann-Whitney U-test (**d**). *P < 0.05, **P < 0.01, ***P < 0.001.

Figure 5. Prenatal vitamin D supplementation protects from asthma development. a, H&E staining of representative lung sections of indicated experimental groups. Arrowheads point to peri bronchial infiltrates. **b-e,** Absolute numbers of total BAL leukocytes (**b**), eosinophils (**c**), lymphocytes (**d**) and lung IL-13+ Th2 cells (**e**). **f**, Flow cytometric analysis of Aiolos expression in differentiating Th2 cells at indicated time

548 points. **g**, QRT-PCR analysis of *Ikzf3* transcripts in respective groups. Expression levels
549 were normalized to the house keeping gene *L32* and are expressed as fold change
550 expression over the control samples WT-vehicle/ WT. **h**, Flow cytometric analysis of
551 Aiolos expression in control and calcitriol stimulated Th2 cells. **i**, Flow cytometric analysis
552 and frequencies of IL-2+ cells in WT and Ikzf3$^{-/-}$ cultures post indicated treatment. Each
553 symbol represents and independent sample (n= 9 per group). Flow cytometric analysis
554 and quantification of VDR expression in lung CD4+ T cells of the respective groups. Each
555 symbol represents one individual mouse and data summarize the results from two to three
556 independent experiments with n>8 per group. Error bars indicate the s.e.m. Statistical
557 significance was determined with Mixed-effect analysis with Holm-Šidák's post-hoc
558 analysis (**b-e**), two-tailed Mann-Whitney U-test (**g, h**) and One-way ANOVA with Holm-
559 Šidák's post-hoc analysis (**g**). *P < 0.05, **P < 0.01, ***P < 0.001, ****P < 0.0001.
560
561 **Extended Data Figure 1: a,** Significant disease and trait associations in 17q21.2 (y-axis),
562 retrieved from the NHGRI-EBI GWAS Catalog, with at least one significant SNPs (x-axis)
563 in Chr17q21.2. Colored bars denote autoimmune diseases mapped to Th1 (red bars) or
564 Th2 (blue bars) driven immunity. **b,** University of California Santa Cruz (UCSC) Genome
565 Browser tracks showing chromosomal location, common dbSNPs, VDR-, RXR-, CTCF-
566 and IKZF3-binding sites and H3K27Ac marks present in the Ch17q21.2 locus. VDR
567 binding sites overlapping with active regulatory elements are highlighted by colored
568 boxes.
569
570 **Extended Data Figure 2. Baseline VDR expression is confined to the CD4+ Foxp3-**
571 **Teff cell population. a**, Gating strategy for the analysis of VDR expression in different
572 leukocyte populations in the lung. **b,** Flow cytometric analysis and cell frequencies of VDR
573 expression in CD45+, CD4+, CD8+ and CD19+ in the respective groups (n=4-5). **c**,
574 Representative flow plots of lung CD45+ CD4+ T cells isolated from saline and HDM-
575 immunized and -challenged mice for the co-expression of Foxp3 and VDR. Each symbol
576 represents one mouse. Numbers in flow plots indicate percentages. Error bars indicate
577 the s.e.m. Statistical tests: two-tailed Mann-Whitney U test. *P < 0.05. Data summarize
578 results from two independent experiments.

Extended Data Figure 3. VDR expression is induced during CD4+ Th2 cell differentiation. a, Representative immunoblot for VDR expression in freshly isolated (0 hrs) and activated CD4+ CD62L+ CD44- naïve T cells (48 hrs.) and *in vitro* polarized Th1, Th2 and iTreg cells. Kidney samples of WT and $VDR^{-/-}$ mice were used as controls. **b**, Representative immunoblot for VDR expression in polarizing Th2 at the indicated days of *in vitro* culture. **c**, Representative image of VDR localization in *in vitro* polarized Th2 cells stimulated with vehicle (EtOH, [% v/v]) or calcitriol.

Extended Data Figure 4. Vitamin D deficiency does not alter CD4+ IL-10 and IL-17A expression allergic airway inflammation. Frequencies of IL-10 (**a**) and IL-17A (**b**) CD4+ T cells. Each symbol represents one mouse. Error bars indicate the s.e.m. Data summarize results from two or three independent experiments with n>8 per group.

Extended Data Figure 5. Flow cytometric analysis and frequencies of IL-13 expression in WT, vitamin D deficient and $VDR^{-/-}$ Th2 cultures (n=5-9 per group). Each symbol represents one individual sample and data summarize the results from two or three independent experiments. Error bars indicate the s.e.m. Statistical tests: Kruskal- Wallis Test with Dunn's post-hoc analysis. *P < 0.05, **P < 0.01, ****P < 0.0001.

Extended Data Figure 6. KEGG pathways analysis post vitamin D stimulation. List of KEGG pathways enriched (p-adj. < 0.05) in DE genes after calcitriol stimulation. The x-axis indicates the number of genes annotated to each pathway. The bar colors indicate the FDR-adjusted p-value based on the colormap on the right side of the figure. The R package clusterProfiler was used for the enrichment analysis and visualization.

Extended Data Figure 7. Active signaling pathways in Th2 cells. a, Schematic representation of the network analysis employed. **b**, Network analysis to visualize active signaling paths in control stimulated Th2 cultures. Predefined set of cell membrane receptors were set as starting points (orange nodes) and annotated transcription factors were set as ending points (blue). All intermediate proteins on the PPI are visualized as

grey nodes. Molecular interactions only overrepresented in control stimulated cells are shown as purple arrows.

Extended Data Figure 8. Prenatal vitamin D supplementation increases VDR expression in CD4+ T cells. a, Schematic presentation of the dietary intervention protocol and breeding scheme with vitamin D. **b**, Flow cytometric analysis and quantification of VDR expression in lung CD4+ T cells of the respective groups. Each symbol represents one individual mouse and data summarize the results from two to three independent experiments with n>8 per group. Error bars indicate the s.e.m. Statistical significance was determined with One-way ANOVA with Holm-Šidák's post-hoc analysis. *P < 0.05, **P < 0.01, ***P < 0.001, ****P < 0.0001.

Extended Data Figure 9. Prenatal vitamin D supplementation mitigates Th2 development and cytokine production *in vitro*. a-g, Representative flow plots and cell frequencies of (**a**) Gata3, (**b**) VDR, (**c**), IL-2, (**d**) IL-13, (**e**) IL-5 expression in indicated groups. Each symbol represents one individual sample and data summarize the results from two to three independent experiments (n= 4-5 per group). Error bars indicate the s.e.m. Statistical test: two-tailed Mann-Whitney U-test (a – g). *P < 0.05, **P < 0.01, ***P < 0.001.

Supplementary Figure 1. Uncropped immunoblot shown in Extended Data Fig. 2a

Supplementary Figure 2. Uncropped immunoblot shown in Extended Data Fig. 2b

Methods

In silico analysis of VDR binding sites on Chr17q12-21

For our *in-silico* analysis, we focused on two genomic regions that are known to harbor variants associated with asthma and autoimmune disease susceptibility. The first one is a 240 kb region that covers parts of the 17q12 and 17q21.1 loci and contains IKZF3, ZPBP2, ORMDL3, GSDMA and GSDMB (chr17: 37,899,254–38,139,253; hg19) and the second one is a 420 kb region in the 17q21.2 locus that includes STAT3, STAT5A and

STAT5B (chr17: 40,330,000-40,750,000; hg19). When selecting these genomic ranges, our criterion was to make the window inclusive of any potential enhancer regions targeting the above genes of interest. We used the GeneHancer [34] track in the UCSC Genome Browser (http://genome.ucsc.edu) to determine predicted enhancer-target gene interactions. We obtained VDR, IKZF3, CTCF and Vitamin D-sensitive CTCF binding sites from [35–38], converted their genomic coordinates to hg19 if a different genome build was used in the original publication, and added them as custom tracks on the Genome Browser. We retrieved the known disease and trait associations in these loci from the NHGRI-EBI GWAS Catalog (downloaded on 7/26/2021) [8] and retained all hits that were deemed significant ($p<10^{-5}$). We downloaded significant single-tissue eQTLs for IKZF3 and PSMCIP3 in all tissues from the Common Fund (CF) Genotype-Tissue Expression Project (GTEx) Analysis Release V8 (dbGaP Accession phs000424.v8.p2), through the GTEx Portal (https://www.gtexportal.org/home/) in July 2021. We calculated linkage disequilibrium (LD) using the NCI LDmatrix Tool (https://ldlink.nci.nih.gov/?tab=ldmatrix), and by selecting all available populations.

Gene expression analysis in VDAART cohort

To understand the putative mechanism linking IKZF3 expression and Vitamin D to asthma risk we considered umbilical cord blood (CB) RNA-seq data from the VDAART trial. Total RNA was isolated from cord blood using the QIAGEN PAXgene Blood RNA Kit according to the manufacturer's protocol. Quality was assessed using the Nanodrop 8000 spectrophotometer. Sequencing libraries were constructed with the TruSeq® Stranded Total RNA Library Prep Globin Kit (Illumina) and the NEXTflex Small RNA sequencing Kit v3 (Boo Scientific). Sequencing was performed using a NextSeq 550 instrument (Illumina). Trimmed reads were mapped to The GRCh38 reference genome using STAR[39]. Read counts were computed with htseq[40]. The data includes 443 expression profiles of pregnant women with and without asthma undergoing measurements of Vitamin D levels in their CB. Each sample is matched with the observed patterns of wheezing and asthma in the newborn. We filtered all the samples where information about Vitamin D levels, asthma/wheezing patterns or other covariates were missing, obtaining

393 expression profiles. Data was normalized with the voom function of the edgeR R package [41], and Vitamin D levels were binarized using 30 ng/ml as threshold. We performed logistic regression of asthma status as a function of the expression levels of IKZF1 and IKZF3, including their interaction term and the interaction between IKZF3 and Vitamin D. Since IKZF3 forms homodimers and heterodimers with IKZF1, we included IKZF1 in the model. We adjusted the model for maternal asthma status and child race.

Mice

All animal studies were approved by the institutional animal care committee. Mice were maintained in a virus- and parasite-free animal facility under a 12-h light, 12-h dark cycle. C57BL6/J wild type (WT) mice were bred and housed at the MGH animal facility. Vitamin D-deficient mice (C57BL6/J) were bred and maintained in a UV-free environment and weaned onto a similar diet lacking vitamin D metabolites (TD97340; Harlan Teklad) that results in undetectable circulating 25-hydroxyvitamin D levels[16]. $VDR^{-/-}$ mice ($Vd^{rtm1Mbd/J}$), on C57BL6/J background, were weaned at 18 d on a diet that maintains normal mineral ion homeostasis in the absence of VDR signaling (2% calcium, 1.25% phosphorus, 20% lactose supplemented diet, TD96348; Harlan Teklad, Madison WI)[42].

BALB/c male and female mice were purchased from Charles River Laboratories at 6–8 weeks of age and fed with diets supplemented with varying amounts of vitamin-D3 (TD97340 was used as base diet and supplemented with either 400 IU vitamin D/kg, 1000 IU vitamin D/kg or 4000 IU vitamin D/kg). Mice were bred on the specific diets for two generations to assure stabilization of vitamin D levels. Resulting F2 litters were used for the experiments. Mice were housed under standard conditions with free access to rodent chow and water. All animal protocols were reviewed and approved by the Harvard Medical School standing committee on animals.

House dust mite induced-airway inflammation.

Mice were exposed to D. pteronyssinus extracts (Greer Laboratories, 10.52 EU/mg endotoxin) via the intranasal application of HDM (25 µg in saline) on days 1,2,3, 8 to 15. Control mice received equal volumes of saline (Hospira Inc., Lake Forest, IL, USA).

Twenty-four hours after the final challenge, mice were sacrificed, and specimens sampled.

Bronchoalveolar Lavage.

Bronchoalveolar Lavage (BAL) was performed with 2 × 1 mL of PBS/0.02% bovine serum albumin (BSA). The total number of leukocytes was determined using a TC20 Automated Cell Counter (BioRad Systems). To differentiate cell types, cytospins were prepared and stained with Kwik-Diff solutions as per manufacturer's instructions (Fisher Scientific) and 200 immune cells per slide were counted.

Histological staining

Lungs were perfusion fixed with zinc fixative (BD Pharmingen, San Diego, CA) Tissues were paraffin embedded, divided into sections, and stained with hematoxylin and eosin by MGH DF/HCC Specialized Histopathology Services Core Histology Core. After paraffin embedment, 3-μm sections were stained with hematoxylin and eosin.

Measurements of serum immunoglobulins

Blood samples were collected 24 hours after the final aerosol challenge and serum was prepared. Total IgE levels were measured by ELISA (Chondrex) according to manufacturer's instructions.

Dissociation of mouse tissues, in vitro polarization of CD4 Th-subsets and flow cytometry analyses.

Lungs were perfused via the right heart ventricle with PBS, excised, and digested with collagenase D (2 mg/ml; Roche) in RPM 1640 (Sigma-Aldrich) for 30 minutes at 37°C. The cell suspension was washed twice with PBS. Erythrocytes were removed by hypotonic lysis. Cells were washed twice with PBS and sieved with 30-μm cell strainers (Miltenyi Biotec). The resulting single cells suspension was used to detect leukocyte populations (CD45 BV421 [clone: 104; Biolegend], CD4 PerCPeFluor710 [RM4-5; eBioscience], CD8a APC-Cy7 [53-6.7; Biolegend], CD19 PE-Cy7 [6D5; Biolegend]) and CD4+ Foxp3+ Treg (CD45 BV421, CD4 PerCPeFluor710, Foxp3 PE [FJK-16s; Thermo

Fisher]), VDR AlexaFluor647 (D2K6W; Cell Signaling Technologies), Aiolos PE (8B2; Biolegend) and cytokine production by Th-cells (see below).

Spleens were excised and mononuclear cells were isolated using a syringe plunger and 100-µm cell strainers. Red blood cells were removed by hypotonic lysis. Tonicity was restored by the addition of RPMI 1640 (Sigma Aldrich). The resulting cell suspension was washed twice with PBS and used for the isolation of naïve CD4+ T cells according to the manufacturer's instructions (Naive T Cell Isolation Kit II; Miltenyi Biotec). Naive CD4+ T cell purity was assessed by staining for CD4 PerCPeFluor710 (clone: RM4-5), CD44 FITC (IM7), and CD62L PE (mel-14).

Naïve T cells were activated with plate bound anti-CD3ε (5 µg/ml, clone: 145-2C11, BD Biosciences) and soluble anti-CD28 (0.5 µg/ml, clone: 37.51, BD Biosciences). Th-subset polarization was induced by exposing naïve CD4+Tcells to following culture conditions for 3 days. Th1 cells: recombinant murine IL-12 (rmIL-12) (10 ng/mL; Peprotech), anti–IL-4 (5 µg/mL; BD Biosciences); Th2 cells: rmIL-4 (20 ng/mL; Peprotech), anti–IFN-γ (5 µg/mL; BD Biosciences), and anti–IL-12 (5 µg/mL; BD Biosciences); Treg: rmTGFβ1 (2 ng/mL; Peprotech), anti–IL-4 (5 µg/mL), anti–IFN-γ (5 µg/mL) for 3 days. Proliferation of Th1 and Th2 cells was induced using rmIL-2 (20 ng/mL; Peprotech) in the presence of Th-polarizing reagents for an additional 2 days. Polarization efficiency was verified by staining for intracellular cytokines (please see below) or Foxp3 expression (see above).

For intracellular cytokine staining, cells were stimulated with phorbol 12-myristate 13-acetate (PMA)/ionomycin and brefeldin A (Cell Stimulation Cocktail; Tonbo Biosiences) for 4 hours. Cells were fixed with Fixation Buffer (Biolegend). Cells were permeabilized using 0.3% saponin in FACS buffer (0.5% FBS in PBS). Antibody staining was performed for 30 minutes in the dark using CD4, IFN-γ (XMG1.2-FITC), IL-10 (JES5-16E3-PE), IL-13 (eBio13A-eFluor660), IL-17A (TC11-18H10.1-PE-Cy7). Cells were washed twice with permeabilization buffer and suspended in FACS buffer. For analysis, 30,000 counts (in the CD4+ gate) were recorded on a FACSFortessa (BD Biosciences) and analyzed with FlowJo software (v10; Tree Star).

765 *Western blot analyses*

766 Cells were lysed in 50 mmol/L Tris/HCl (pH 7.5), 150 mmol/L NaCl, 1% NP-40, and 1×
767 protease and phosphatase inhibitor mix (both Roche) for 15 minutes on ice. Lysates were
768 clarified, and total protein concentrations were measured with BCA (Pierce). Proteins (20
769 µg) were separated on gradient gels (Mini-PROTEAN® TGX; BioRad) and transferred on
770 a Immun-Blot PVDF membrane (BioRad). Unspecific binding was blocked using 5 % milk
771 powder in TBST for 30 min. Anti-VDR (D2K6W, 1:1000; Cell Signaling Technologies,
772 CST) was incubated in 0.5 % milk powder in TBST overnight at 4° C. Membranes were
773 washed 3 times with TBST and incubated with secondary anti-rabbit IgG, HRP-linked
774 Antibody (#7074; CST) for 2 hours. To control for equal loading, membranes was probed
775 for β-actin (AC-15; 1:10,000; Sigma-Aldrich) expression for 2 hrs. at RT. Protein bands
776 were visualized with Luminol reagent (Pierce) using the ChemiDoc XRS+system
777 (BioRad).

778

779 *Immunofluorescence staining for confocal microscopy*

780 *In vitro* polarized Th2 cells (see above) were stimulated with 100 nm calcitriol (in ethanol)
781 or ethanol [equal v/v] for the final 24 hrs of culture. Cells were washed twice with PBS
782 and spun onto poly-L-lysine coated glass slides. After drying, cells were fixed with 4 %
783 PFA in PBS for 15 min. Cells were permeabilized using 0.2% Triton X-100 in PBS for 20
784 min. Cells were washed 3 times for 5 min with PBS and incubated with Image-iT FX Signal
785 Enhancer (Thermo Fisher Scientific) for 30 min at RT. After three consecutive washes
786 with PBS, unspecific binding was blocked using blocking buffer (PBS/5 % goat serum/0.3
787 % Triton X-100) for 60 min at RT. Primary antibodies directed against CD4-FITC (clone;
788 1:100, BD Biosciences), VDR (D2K6W; 1: 200, CST) were incubated in a humidified
789 chamber over night at 4° C. After 3 washes with PBS, slides were incubated with the
790 secondary reagent, anti-rabbit-Cy3 (1:500; Thermo) for 30 min at RT in the dark. After
791 three more washes with PBS, slides were mounted with ProLong Gold with DAPI
792 according to manufacturer's instructions (Invitrogen). Images were acquired in a single
793 z-plane using a Zeiss immunofluorescence microscope with a 40x objective.

794

795 *Total RNA isolation, quality control, and RNA-sequencing analysis*.

Total RNA was isolated using TRIzol™ Reagent (Invitrogen) according to the manufacturer's instructions. Quality was assessed using the Nanodrop 8000 spectrophotometer. Sequencing libraries were constructed with the TruSeq® Stranded Total RNA Library Prep Globin Kit (Illumina). Sequencing was performed using a HiSeq. 2500 instrument (Illumina). Trimmed reads were mapped to the GRCm38 reference genome using STAR[39]. Read counts were computed with htseq[40]. Data were normalized and differential expression was analyzed with the R package DESeq2 (v.1.34.0) [43] using a false discovery rate (FDR) < 0.05.

Pathway enrichment, Overrepresentation and Gene Set Enrichment analysis.

KEGG pathway, overrepresentation and gene set enrichment analyses were performed with the "enrichKEGG", "enrichr" and "GSEA" function in the R package "clusterProfiler" (v.3.10.1) with default settings [44]. P-values were adjusted using the BH-FDR correction and enriched terms with a p-adj.<0.05 selected.

Network analysis

RNA-Sequencing data extracted from murine Th2 cells were analyzed using the R package DESeq2 (v.1.22.2) [43]. Raw counts were normalized and transformed for variance stabilization using the DESeq2 function rlog (regularized-logarithm transformation). Batch effects were removed using the function removeBatchEffect of the R package LIMMA[45]. Gene with counts lower than 5 in at least one sample were removed for downstream analyses.

Differential expression analysis was performed between control Th2 cells versus calcitriol stimulated Th2 cells using DeSeq2 [43]. The design matrix was built to consider batch effects derived from the RNA isolation process. DESeq2-independent filtering was applied [43] and P values were corrected for multiple hypothesis testing by using the Benjamini-Hochberg (BH)-FDR adjustment [46].

The PPI network used in our network analysis was developed by Silverbush et al. [17]. As described in the original paper, this human PPI network was reconstructed by integrating

large scale PPI databases, drug response repositories, and cancer genomics data. Only the largest connected component of the network was considered, resulting in an interactome of 15,500 proteins and 234,585 consensus-oriented interactions. Conversion between murine and human gene IDs was performed using the BioMart conversion tool [47]. We also assumed a one-to-one correspondence between genes and their protein products in the entire analysis.

To identify the active signaling paths in control and calcitriol stimulated Th2 cells, we modelled the transmission of the molecular signal as a sequential path on the PPI network (called a network path) that starts from a receptor, connects the receptor to multiple intermediate proteins, and leads to a transcription factor. Receptors and transcription factors were selected from a predefined list based on their role in Th2 cell biology and IL-2 expression (Extended Data Table 8). CD3, CD28, IL-4R, IL-13R were selected based on their role in Th2 differentiation. The IL-2R complex was included due to being a target of vitamin D signaling. TGFβRs were selected based on the immunomodulatory activity of this signaling path in CD4+ T cells. role in mediating immunoregulation. Using this subset of receptors and transcription factors as input for the implementation of our network analysis, we computed all the shortest paths connecting each receptor-transcription factor pair on the PPI network. For both control and calcitriol stimulated Th2 cells, we ranked each network path based on the average expression of the path's nodes. The top selected paths represent the most active downstream processes in Th2 cells in each condition.

mRNA isolation, reverse transcription, and real-time RT-PCR.

Total RNA from in vitro polarized Th2 cells was isolated with the RNeasy Mini Kit (Qiagen). First-strand cDNA synthesis was performed with the Omniscript kit (Qiagen). Quantitative real-time PCR was performed with the SsoFast EvaGreen Supermix Kit (BioRad) on a AriaMx Real-time PCR System (Agilent) as per manufacturer's instructions. Primers sequences used in this study are listed in Extended Data Table 9. Relative gene expression levels were calculated with the $2^{-\Delta\Delta Ct}$ method, with normalization to the murine ribosomal L32 as the housekeeping gene. Data are presented as fold induction over the

858 respective control groups (vehicle or WT). All standard procedures were performed
859 according to the manufacturer's instructions.
860
861 Quantification and statistical analysis.
862 For each figure the number of replicates per experiment is indicated in the corresponding
863 figure legend. In the figures, mean and standard error of the mean (s.e.m.) are presented
864 and error bars represent the mean ± s.e.m. Two group comparisons were analyzed using
865 unpaired two-tailed Student's t-tests (parametric data) and Mann–Whitney U-test (non-
866 parametric data). Multiple group comparisons were analyzed with Kruskal-Wallis and
867 One-way ANOVA test with Tukey's post hoc analysis. *In vivo* experiments were analyzed
868 using Mixed-effect analysis or Two-way ANOVA test with Holm-Šidák's post-hoc analysis
869 (factors: genotype & exposure, diet & exposure). Prism 9.2 (GraphPad Software) was
870 used to calculate statistics. P values of less than 0.05 were considered statistically
871 significant.
872
873 **Acknowledgements:** We wish to thank the VDAART trial participants and clinical staff
874 for their critical work on the VDAART study. We wish to thank our Channing colleagues
875 for comments, the National Heart Lung and Blood institute for funding via 5P01HL132825,
876 5UH3OD023268 and 5K25HL150336, and the German Society for Clinical Chemistry and
877 Laboratory Medicine (DGKL) and the German Research Foundation (DFG) for funding
878 via KI 1868/3-1.
879
880 **Author information:** These authors jointly supervised this work: Ayşe Kılıç, Scott T.
881 Weiss
882
883 **Contributions**
884 A.K. and S.T.W. designed the experiments, analyzed data, and wrote the manuscript.
885 A.K., M.G.D., T.R.B., J.R.Q., A.O.S, J.K., T.N., H.Y.P., N.K. and R.E.A performed
886 experiments. A.H., E.M., M.D.M. and R. C. analyzed data. M.D. and K.G. provided critical
887 mouse lines and scientific input. A.A.L. assisted on VDAART related analyses. H.R. and

B.D.L. supervised experiments and provided critical scientific input. All authors critically reviewed the manuscript.

Ethics declarations: none

Competing interest

Dr. Weiss receives royalties from UpToDate and is an investor in Histolix. All other authors declare no competing interests.

Supplementary Information is available for this paper.

Correspondence and requests for materials should be addressed to Ayşe Kılıç and Scott T. Weiss

Peer review information

Reprints and permissions information is available at www.nature.com/reprints.

References

1. Litonjua, A. A. & Weiss, S. T. Is vitamin D deficiency to blame for the asthma epidemic? *The Journal of allergy and clinical immunology* **120,** 1031–1035; 10.1016/j.jaci.2007.08.028 (2007).
2. Bouzigon, E. *et al.* Effect of 17q21 variants and smoking exposure in early-onset asthma. *The New England journal of medicine* **359,** 1985–1994; 10.1056/NEJMoa0806604 (2008).
3. Kelly, R. S. *et al.* The role of the 17q21 genotype in the prevention of early childhood asthma and recurrent wheeze by vitamin D. *The European respiratory journal* **54**; 10.1183/13993003.00761-2019 (2019).
4. Schmiedel, B. J. *et al.* 17q21 asthma-risk variants switch CTCF binding and regulate IL-2 production by T cells. *Nature communications* **7,** 13426; 10.1038/ncomms13426 (2016).
5. Moffatt, M. F. *et al.* Genetic variants regulating ORMDL3 expression contribute to the risk of childhood asthma. *Nature* **448,** 470–473; 10.1038/nature06014 (2007).
6. Litherland, S. A. *et al.* Signal transduction activator of transcription 5 (STAT5) dysfunction in autoimmune monocytes and macrophages. *Journal of autoimmunity* **24,** 297–310; 10.1016/j.jaut.2005.02.001 (2005).
7. Kara, S., Pirela-Morillo, G. A., Gilliam, C. T. & Wilson, G. D. Identification of novel susceptibility genes associated with seven autoimmune disorders using whole genome

molecular interaction networks. *Journal of autoimmunity* **97,** 48–58; 10.1016/j.jaut.2018.10.002 (2019).

8. Buniello, A. *et al.* The NHGRI-EBI GWAS Catalog of published genome-wide association studies, targeted arrays and summary statistics 2019. *Nucleic acids research* **47,** D1005-D1012; 10.1093/nar/gky1120 (2019).
9. Syreeni, A. *et al.* Genome-wide search for genes affecting the age at diagnosis of type 1 diabetes. *Journal of internal medicine* **289,** 662–674; 10.1111/joim.13187 (2021).
10. Shrine, N. *et al.* Moderate-to-severe asthma in individuals of European ancestry: a genome-wide association study. *The Lancet. Respiratory medicine* **7,** 20–34; 10.1016/S2213-2600(18)30389-8 (2019).
11. Marinho, S., Custovic, A., Marsden, P., Smith, J. A. & Simpson, A. 17q12-21 variants are associated with asthma and interact with active smoking in an adult population from the United Kingdom. *Annals of allergy, asthma & immunology : official publication of the American College of Allergy, Asthma, & Immunology* **108,** 402-411.e9; 10.1016/j.anai.2012.03.002 (2012).
12. Hitomi, Y. *et al.* Identification of the functional variant driving ORMDL3 and GSDMB expression in human chromosome 17q12-21 in primary biliary cholangitis. *Scientific reports* **7,** 2904; 10.1038/s41598-017-03067-3 (2017).
13. Keshari, P. K. *et al.* Allelic imbalance of multiple sclerosis susceptibility genes IKZF3 and IQGAP1 in human peripheral blood. *BMC genetics* **17,** 59; 10.1186/s12863-016-0367-4 (2016).
14. Verlaan, D. J. *et al.* Allele-specific chromatin remodeling in the ZPBP2/GSDMB/ORMDL3 locus associated with the risk of asthma and autoimmune disease. *American journal of human genetics* **85,** 377–393; 10.1016/j.ajhg.2009.08.007 (2009).
15. Devereux, G. *et al.* Maternal vitamin D intake during pregnancy and early childhood wheezing. *The American journal of clinical nutrition* **85,** 853–859; 10.1093/ajcn/85.3.853 (2007).
16. Sakai, Y., Kishimoto, J. & Demay, M. B. Metabolic and cellular analysis of alopecia in vitamin D receptor knockout mice. *The Journal of clinical investigation* **107,** 961–966; 10.1172/JCI11676 (2001).
17. Silverbush, D. & Sharan, R. A systematic approach to orient the human protein-protein interaction network. *Nature communications* **10,** 3015; 10.1038/s41467-019-10887-6 (2019).
18. Quintana, F. J. *et al.* Aiolos promotes TH17 differentiation by directly silencing Il2 expression. *Nature immunology* **13,** 770–777; 10.1038/ni.2363 (2012).
19. Raby, B. A. *et al.* Association of vitamin D receptor gene polymorphisms with childhood and adult asthma. *American journal of respiratory and critical care medicine* **170,** 1057–1065; 10.1164/rccm.200404-447OC (2004).
20. Camargo, C. A. *et al.* Maternal intake of vitamin D during pregnancy and risk of recurrent wheeze in children at 3 y of age. *The American journal of clinical nutrition* **85,** 788–795; 10.1093/ajcn/85.3.788 (2007).
21. van der Pligt, P. *et al.* Associations of Maternal Vitamin D Deficiency with Pregnancy and Neonatal Complications in Developing Countries: A Systematic Review. *Nutrients* **10**; 10.3390/nu10050640 (2018).
22. Roth, D. E. *et al.* Global prevalence and disease burden of vitamin D deficiency: a roadmap for action in low- and middle-income countries. *Annals of the New York Academy of Sciences* **1430,** 44–79; 10.1111/nyas.13968 (2018).

23. Cashman, K. D. Vitamin D Deficiency: Defining, Prevalence, Causes, and Strategies of Addressing. *Calcified tissue international* **106,** 14–29; 10.1007/s00223-019-00559-4 (2020).
24. Litonjua, A. A. *et al.* The Vitamin D Antenatal Asthma Reduction Trial (VDAART): rationale, design, and methods of a randomized, controlled trial of vitamin D supplementation in pregnancy for the primary prevention of asthma and allergies in children. *Contemporary clinical trials* **38,** 37–50; 10.1016/j.cct.2014.02.006 (2014).
25. Litonjua, A. A. *et al.* Effect of Prenatal Supplementation With Vitamin D on Asthma or Recurrent Wheezing in Offspring by Age 3 Years: The VDAART Randomized Clinical Trial. *JAMA* **315,** 362–370; 10.1001/jama.2015.18589 (2016).
26. Litonjua, A. A. *et al.* Six-Year Follow-up of a Trial of Antenatal Vitamin D for Asthma Reduction. *The New England journal of medicine* **382,** 525–533; 10.1056/NEJMoa1906137 (2020).
27. Wolsk, H. M. *et al.* Prenatal vitamin D supplementation reduces risk of asthma/recurrent wheeze in early childhood: A combined analysis of two randomized controlled trials. *PloS one* **12,** e0186657; 10.1371/journal.pone.0186657 (2017).
28. Wolsk, H. M. *et al.* Vitamin D supplementation in pregnancy, prenatal 25(OH)D levels, race, and subsequent asthma or recurrent wheeze in offspring: Secondary analyses from the Vitamin D Antenatal Asthma Reduction Trial. *The Journal of allergy and clinical immunology* **140,** 1423-1429.e5; 10.1016/j.jaci.2017.01.013 (2017).
29. Miller, M. *et al.* ORMDL3 transgenic mice have increased airway remodeling and airway responsiveness characteristic of asthma. *Journal of immunology (Baltimore, Md. : 1950)* **192,** 3475–3487; 10.4049/jimmunol.1303047 (2014).
30. Zhang, Y. *et al.* The ORMDL3 Asthma Gene Regulates ICAM1 and Has Multiple Effects on Cellular Inflammation. *American journal of respiratory and critical care medicine* **199,** 478–488; 10.1164/rccm.201803-0438OC (2019).
31. Pfeffer, P. E. & Hawrylowicz, C. M. Vitamin D in Asthma: Mechanisms of Action and Considerations for Clinical Trials. *Chest* **153,** 1229–1239; 10.1016/j.chest.2017.09.005 (2018).
32. Baeke, F. *et al.* Human T lymphocytes are direct targets of 1,25-dihydroxyvitamin D3 in the immune system. *The Journal of steroid biochemistry and molecular biology* **121,** 221–227; 10.1016/j.jsbmb.2010.03.037 (2010).
33. Zhu, J., Cote-Sierra, J., Guo, L. & Paul, W. E. Stat5 activation plays a critical role in Th2 differentiation. *Immunity* **19,** 739–748; 10.1016/s1074-7613(03)00292-9 (2003).
34. Fishilevich, S. *et al.* GeneHancer: genome-wide integration of enhancers and target genes in GeneCards. *Database : the journal of biological databases and curation* **2017**; 10.1093/database/bax028 (2017).
35. Neme, A., Seuter, S. & Carlberg, C. Vitamin D-dependent chromatin association of CTCF in human monocytes. *Biochimica et biophysica acta* **1859,** 1380–1388; 10.1016/j.bbagrm.2016.08.008 (2016).
36. Neme, A., Seuter, S. & Carlberg, C. Selective regulation of biological processes by vitamin D based on the spatio-temporal cistrome of its receptor. *Biochimica et biophysica acta. Gene regulatory mechanisms* **1860,** 952–961; 10.1016/j.bbagrm.2017.07.002 (2017).
37. Ramagopalan, S. V. *et al.* A ChIP-seq defined genome-wide map of vitamin D receptor binding: associations with disease and evolution. *Genome research* **20,** 1352–1360; 10.1101/gr.107920.110 (2010).

38. Lu, X. *et al.* MTA2/NuRD Regulates B Cell Development and Cooperates with OCA-B in Controlling the Pre-B to Immature B Cell Transition. *Cell reports* **28,** 472-485.e5; 10.1016/j.celrep.2019.06.029 (2019).
39. Dobin, A. *et al.* STAR: ultrafast universal RNA-seq aligner. *Bioinformatics (Oxford, England)* **29,** 15–21; 10.1093/bioinformatics/bts635 (2013).
40. Anders, S., Pyl, P. T. & Huber, W. HTSeq--a Python framework to work with high-throughput sequencing data. *Bioinformatics (Oxford, England)* **31,** 166–169; 10.1093/bioinformatics/btu638 (2015).
41. McCarthy, D. J., Chen, Y. & Smyth, G. K. Differential expression analysis of multifactor RNA-Seq experiments with respect to biological variation. *Nucleic acids research* **40,** 4288–4297; 10.1093/nar/gks042 (2012).
42. Li, Y. C. *et al.* Normalization of mineral ion homeostasis by dietary means prevents hyperparathyroidism, rickets, and osteomalacia, but not alopecia in vitamin D receptor-ablated mice. *Endocrinology* **139,** 4391–4396; 10.1210/endo.139.10.6262 (1998).
43. Love, M. I., Huber, W. & Anders, S. Moderated estimation of fold change and dispersion for RNA-seq data with DESeq2. *Genome biology* **15,** 550; 10.1186/s13059-014-0550-8 (2014).
44. Yu, G., Wang, L.-G., Han, Y. & He, Q.-Y. clusterProfiler: an R package for comparing biological themes among gene clusters. *Omics : a journal of integrative biology* **16,** 284–287; 10.1089/omi.2011.0118 (2012).
45. Ritchie, M. E. *et al.* limma powers differential expression analyses for RNA-sequencing and microarray studies. *Nucleic acids research* **43,** e47; 10.1093/nar/gkv007 (2015).
46. Benjamini, Y., Drai, D., Elmer, G., Kafkafi, N. & Golani, I. Controlling the false discovery rate in behavior genetics research. *Behavioural brain research* **125,** 279–284; 10.1016/s0166-4328(01)00297-2 (2001).
47. Smedley, D. *et al.* The BioMart community portal: an innovative alternative to large, centralized data repositories. *Nucleic acids research* **43,** W589-98; 10.1093/nar/gkv350 (2015).

Figure 1

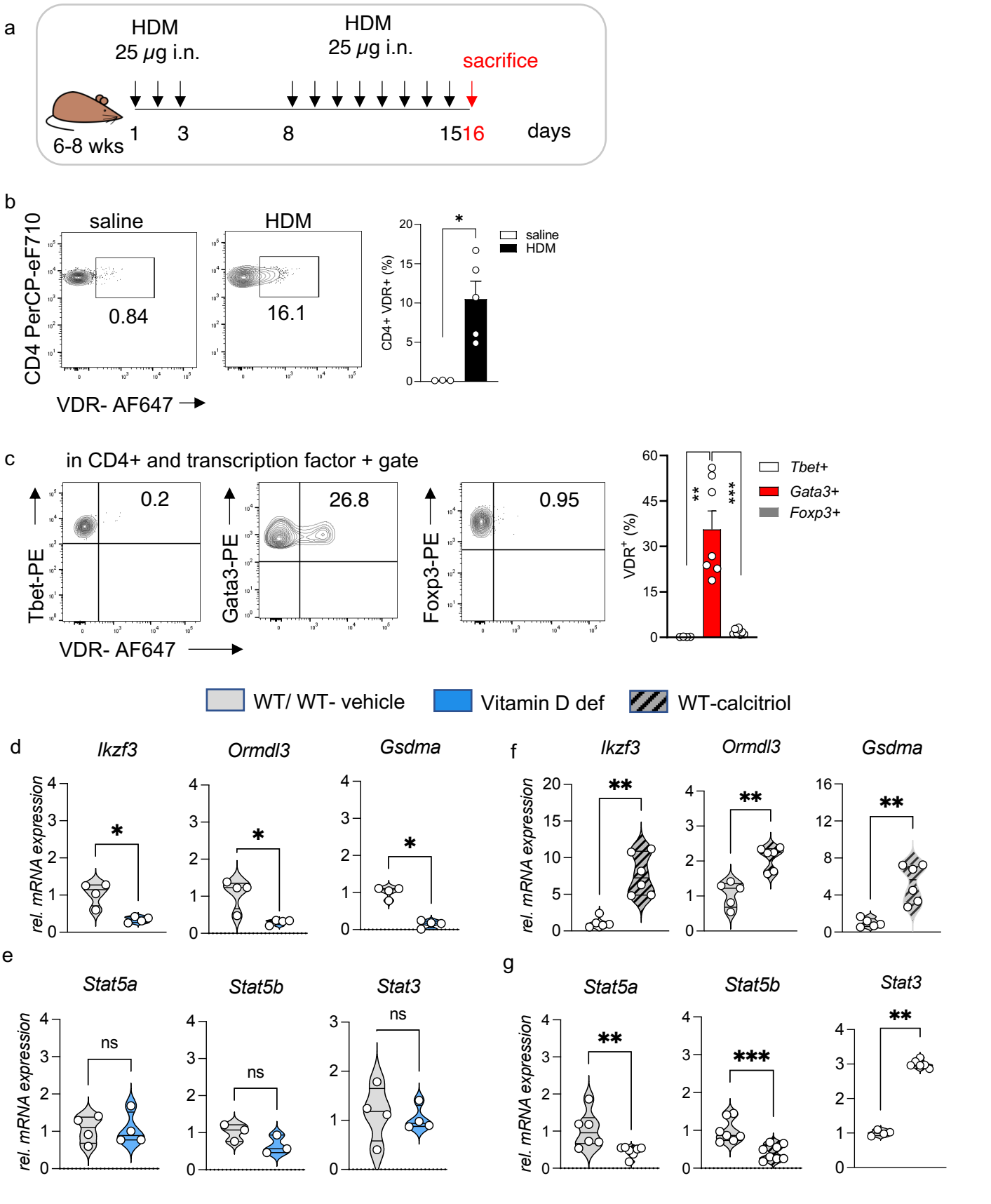

Figure 2

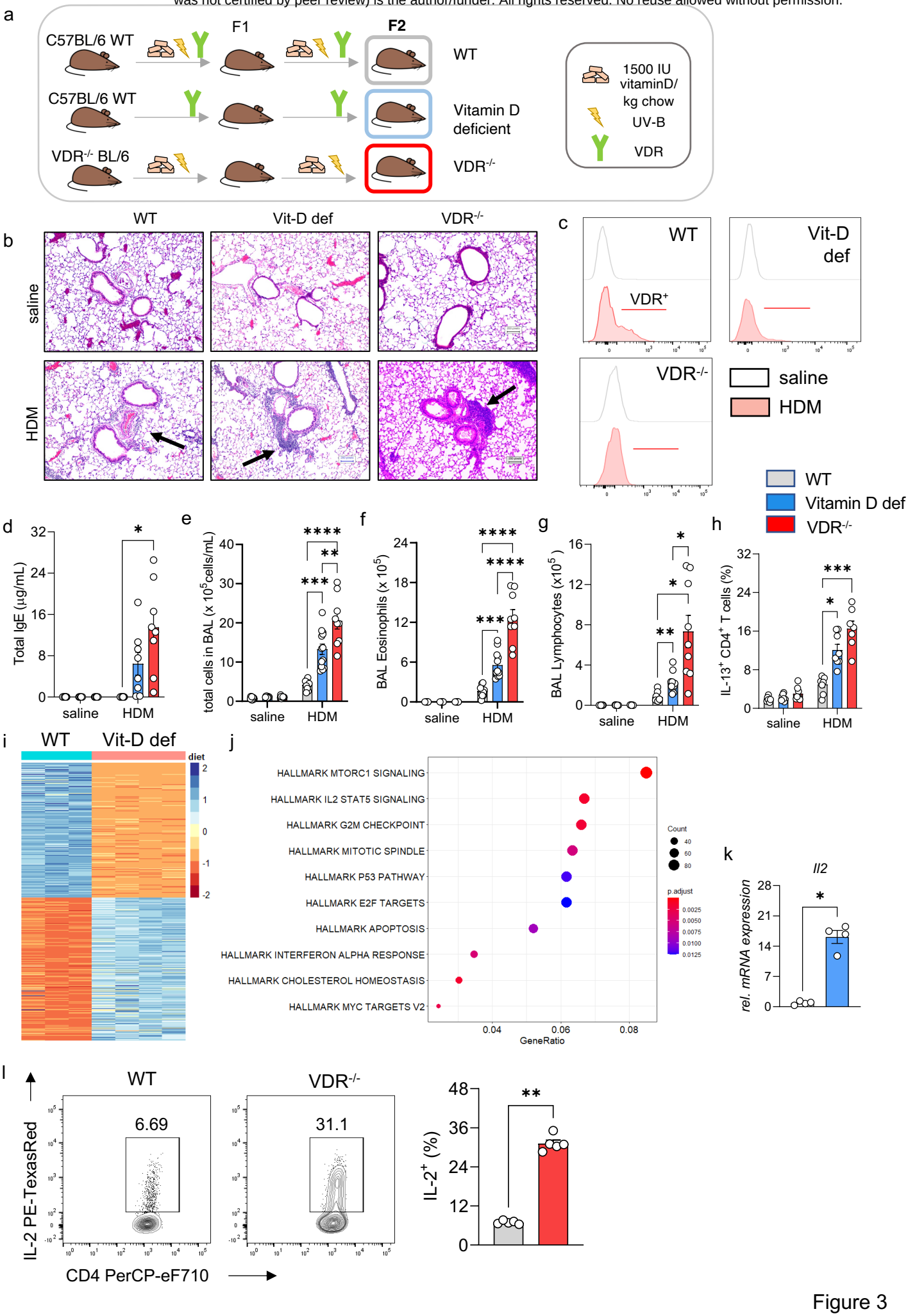

Figure 3

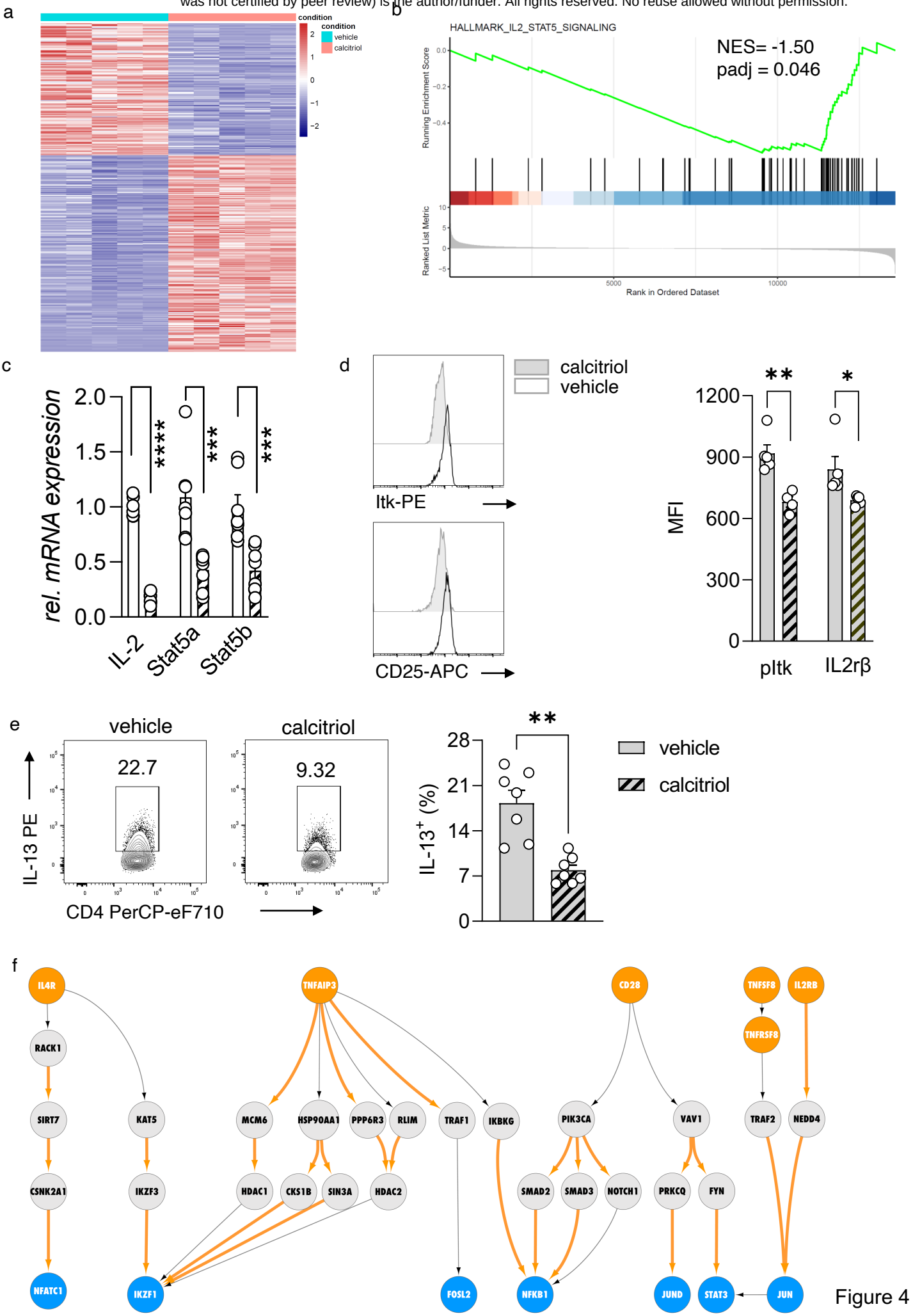

Figure 4

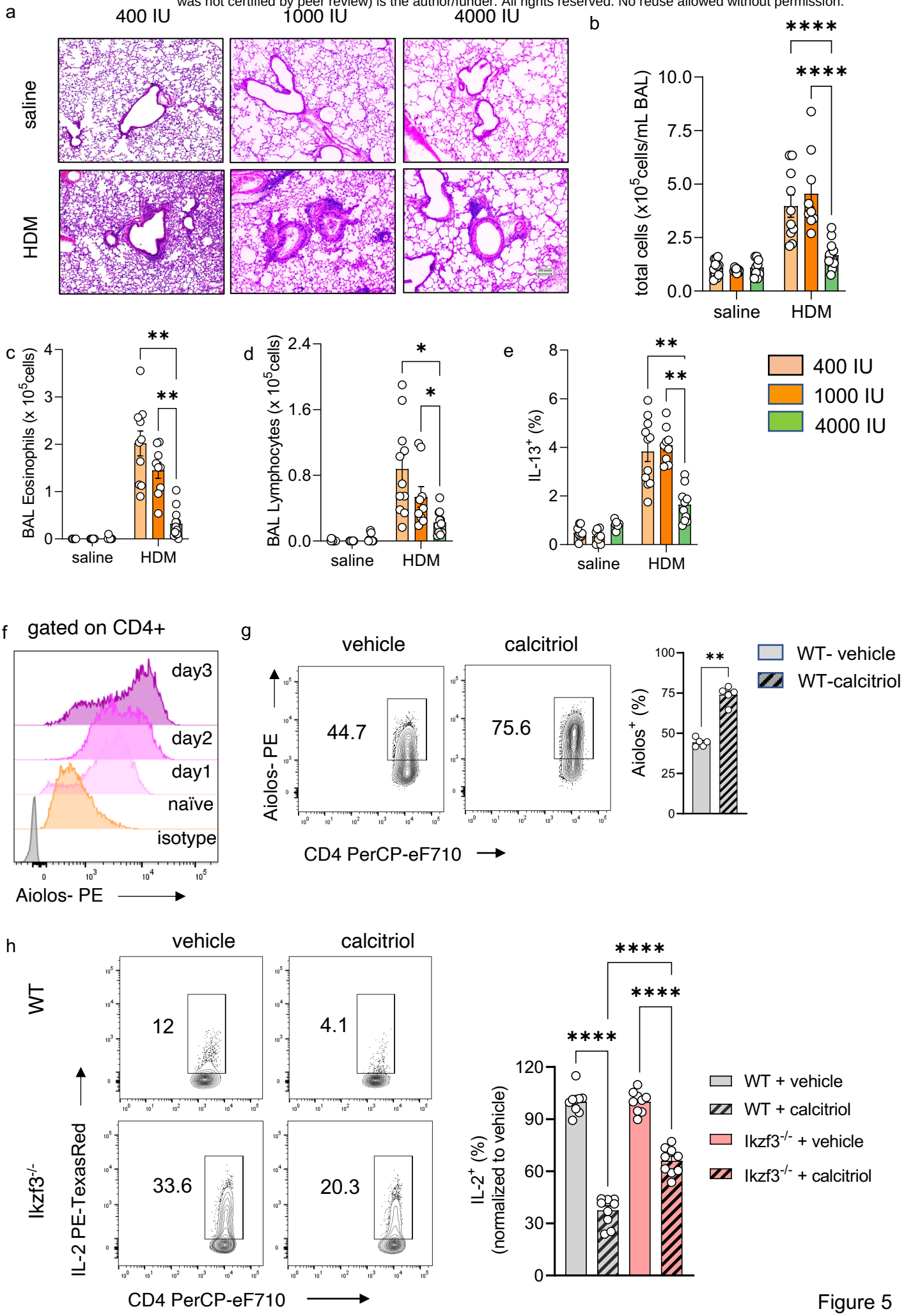

Figure 5

a

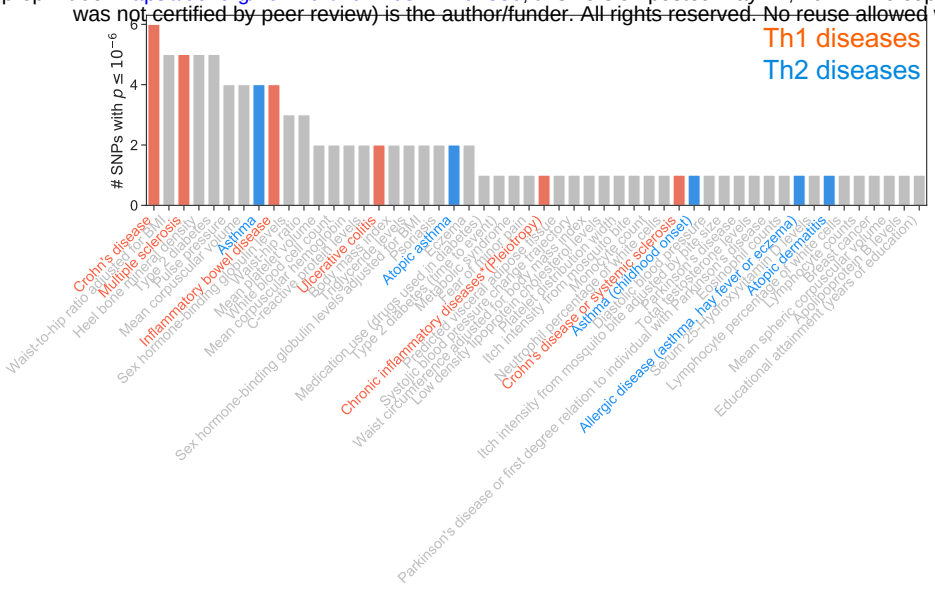

b

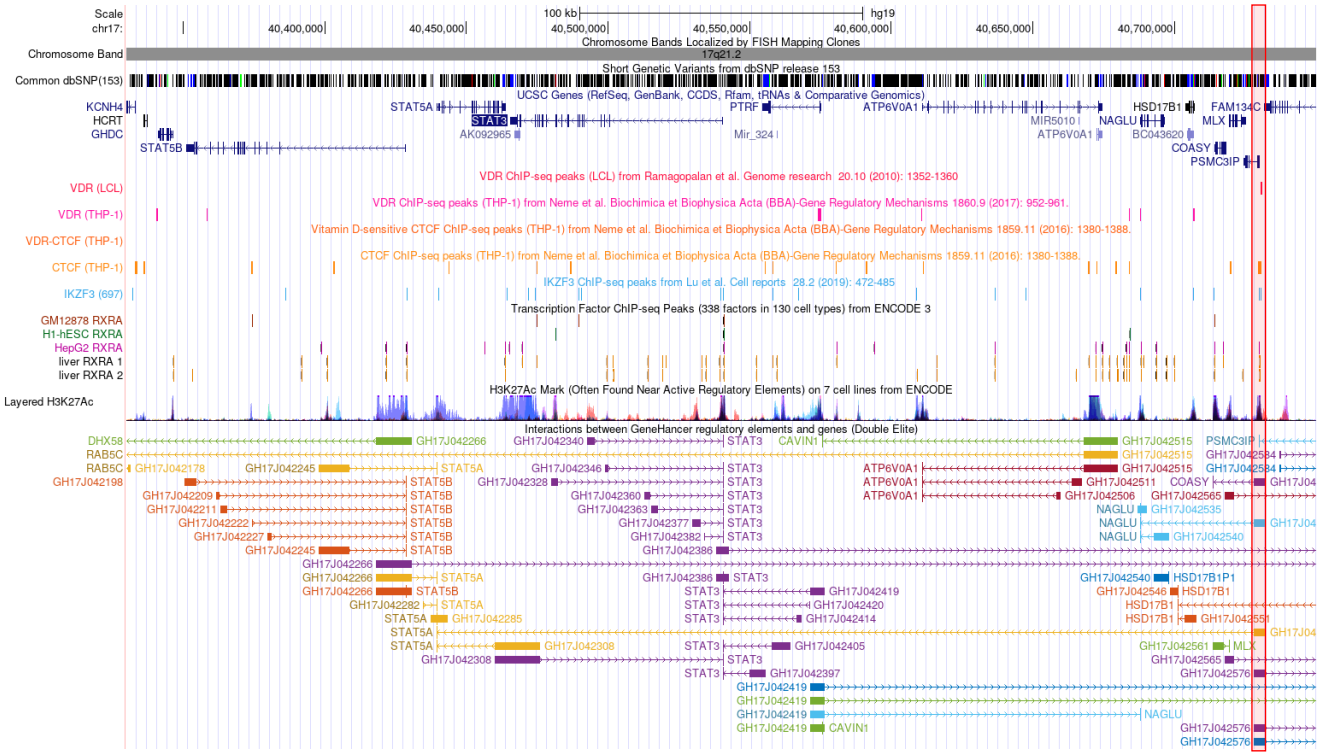

Extended Data Figure 1

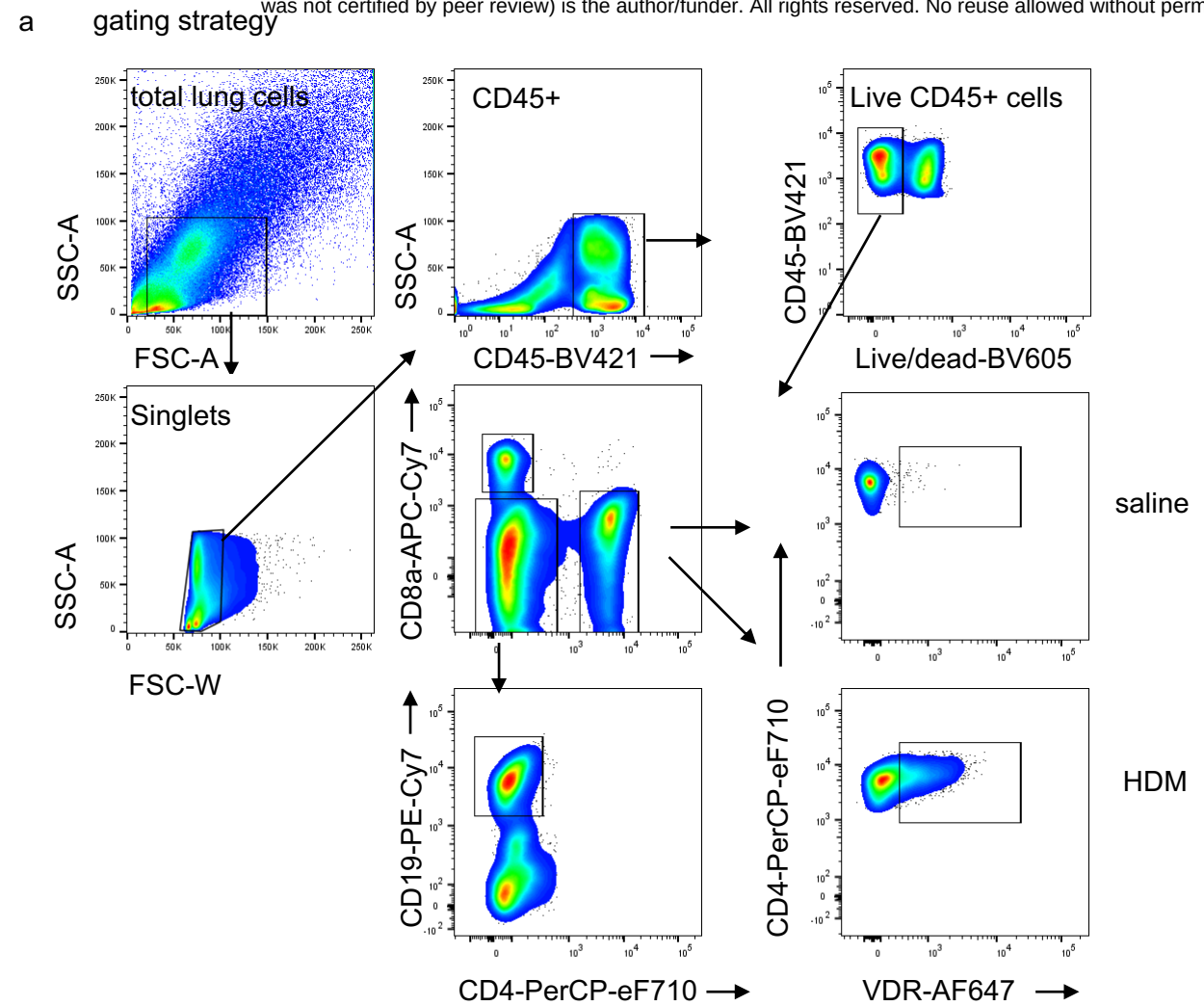

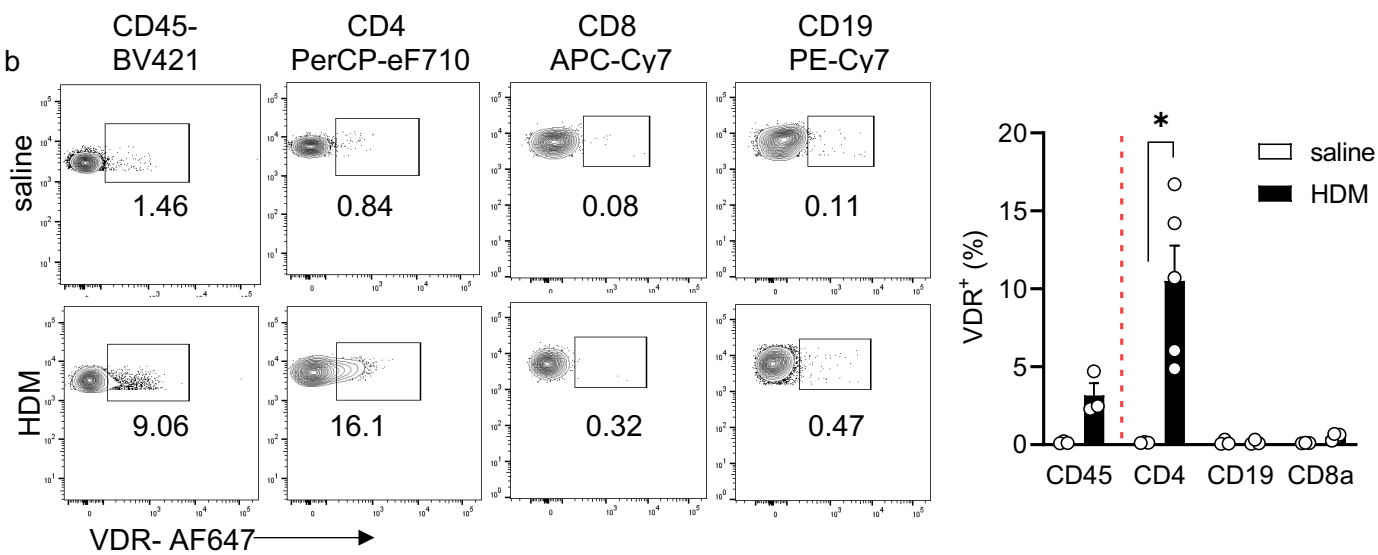

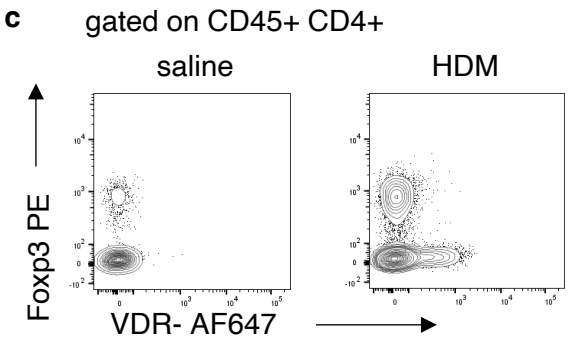

Extended Data Figure 2

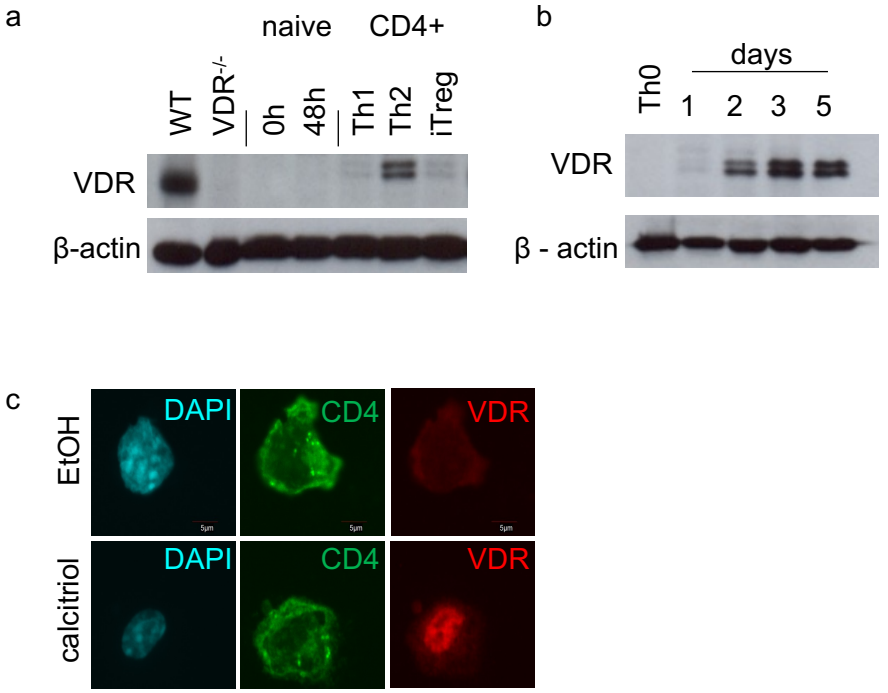

Extended Data Figure 3

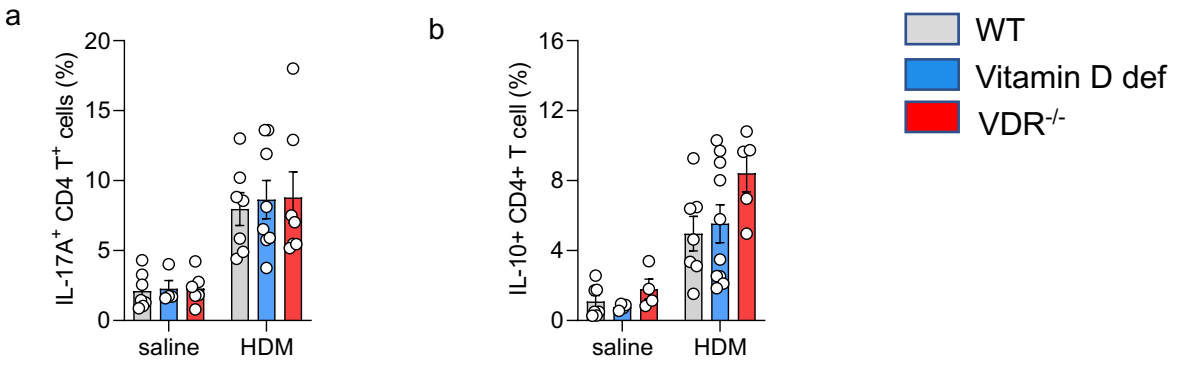

Extended Data Figure 4

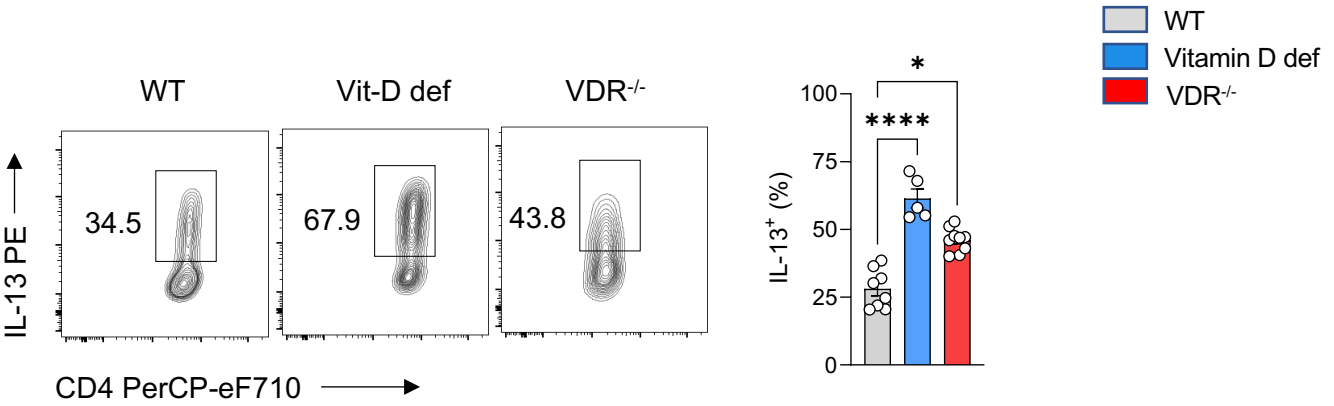

Extended Data Figure 5

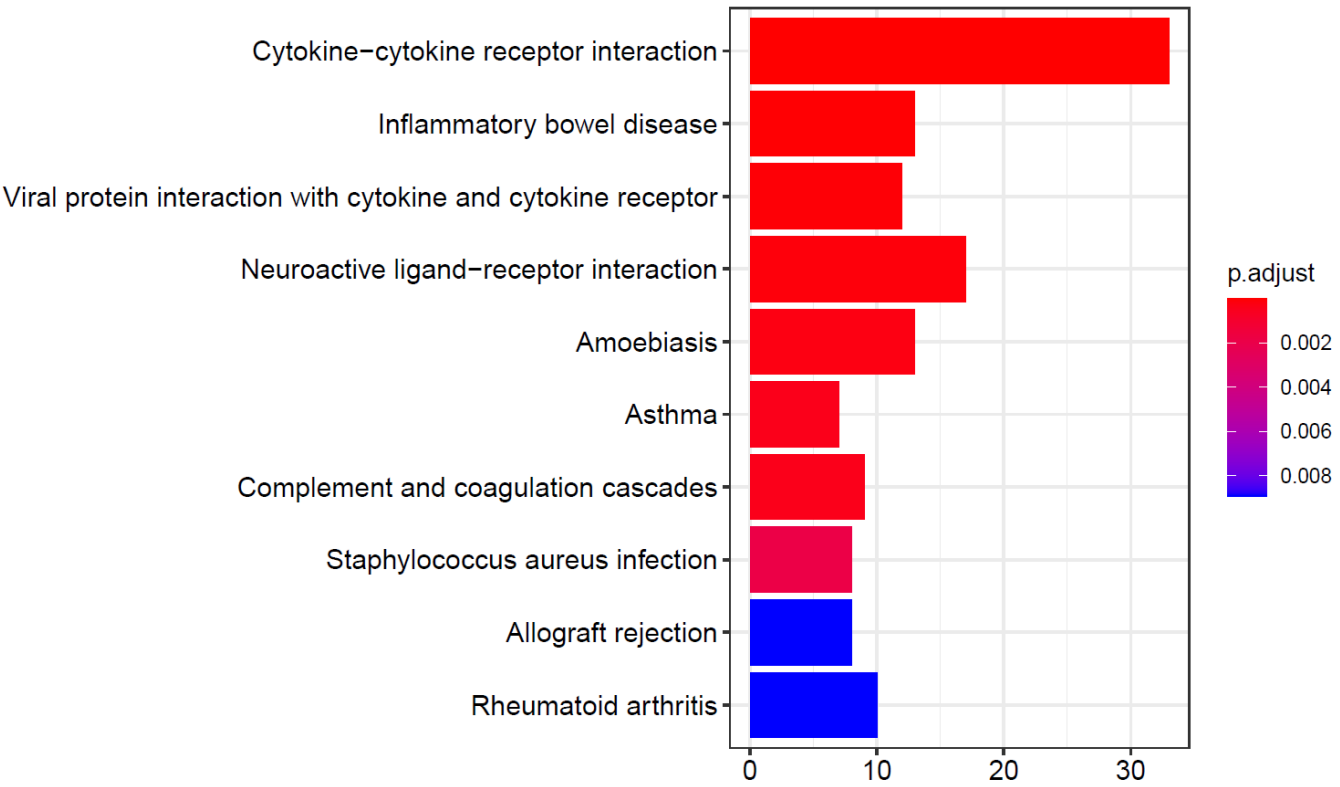

Extended Data Figure 6

a

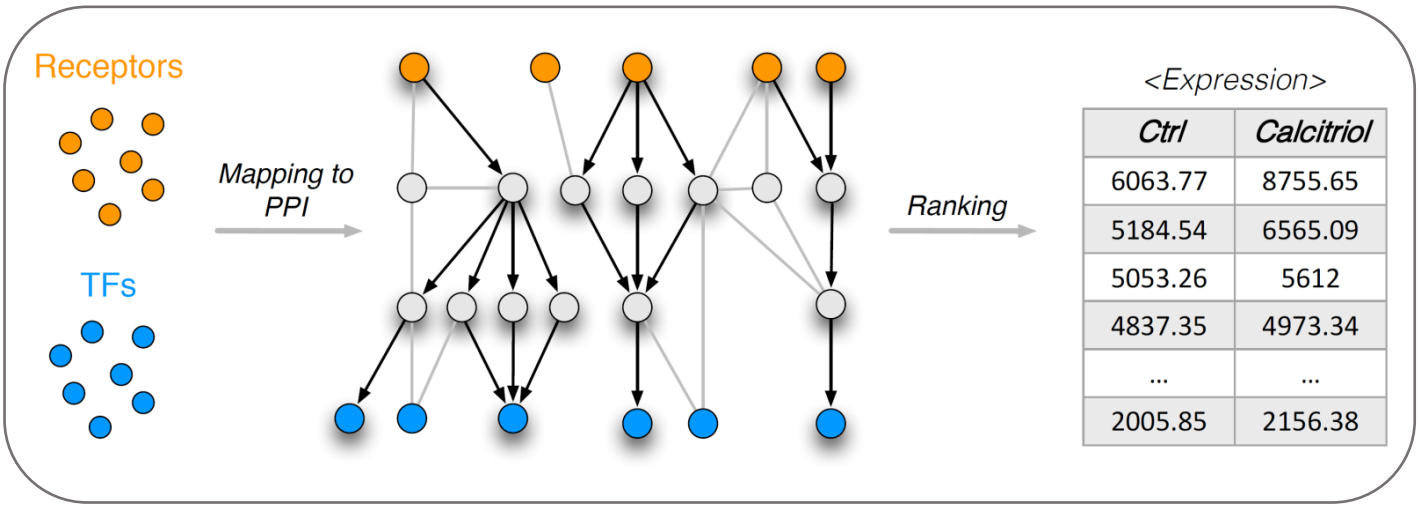

b

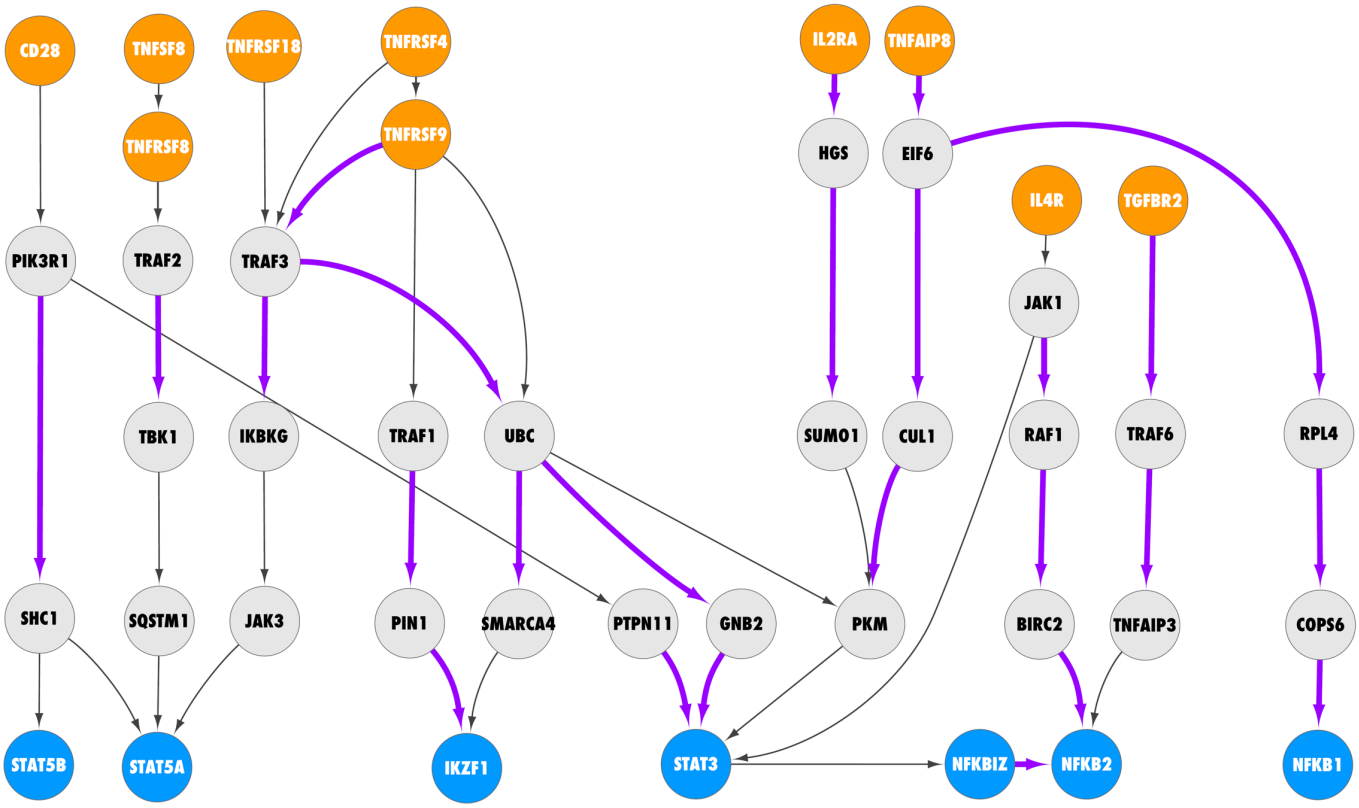

Extended Data Figure 7

a

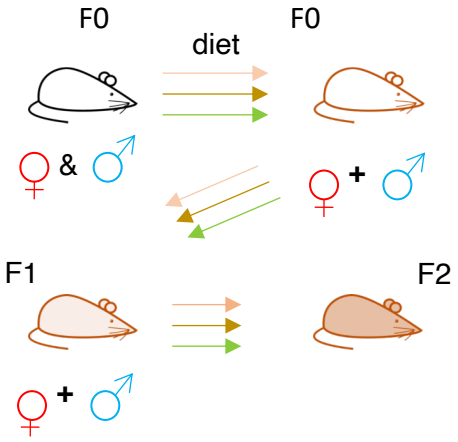

diets:
400 IU (low) /
1000 IU (regular)/
4000 IU (high)
Vitamin D / kg chow

b

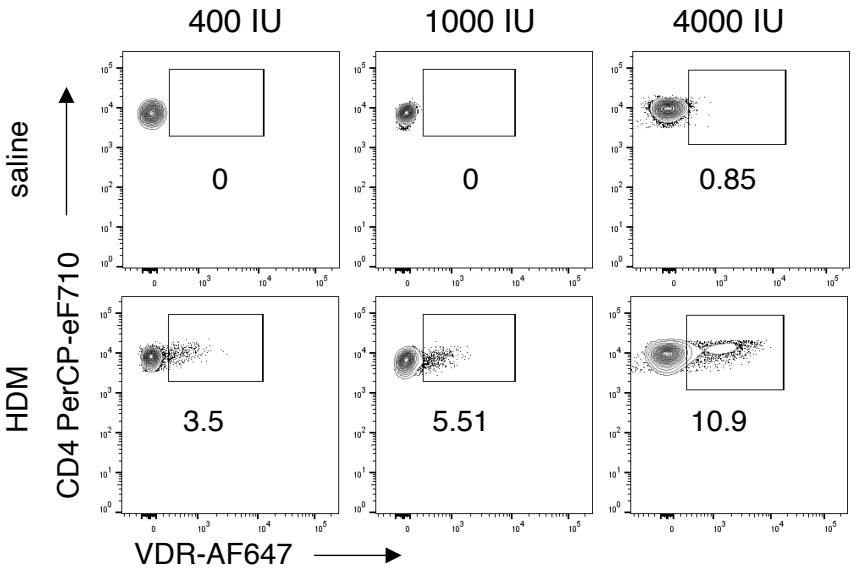

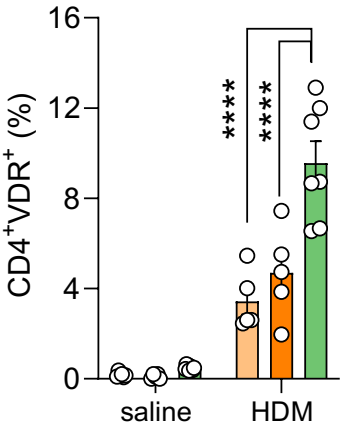

Extended Data Figure 8

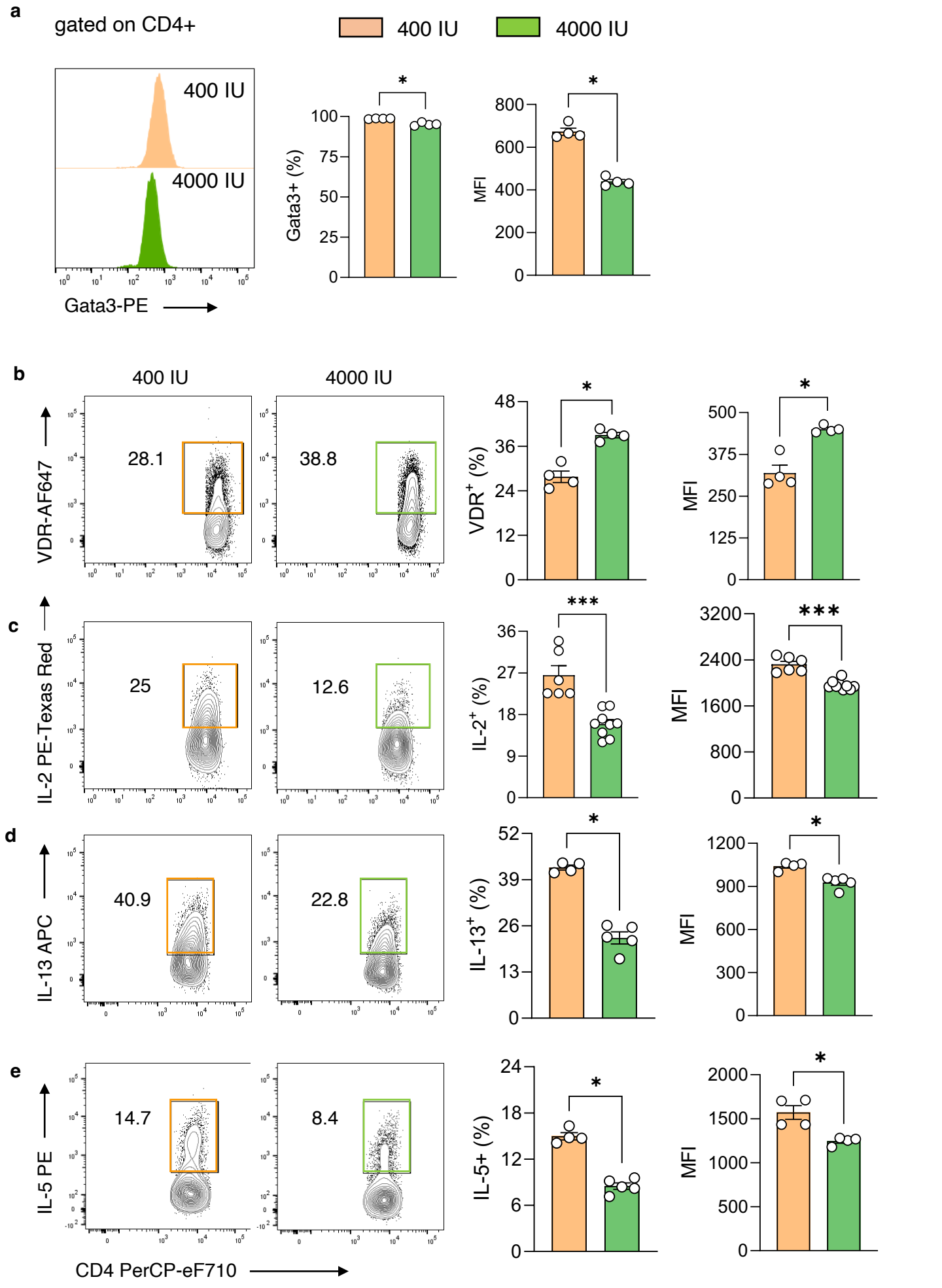

Extended Data Figure 9

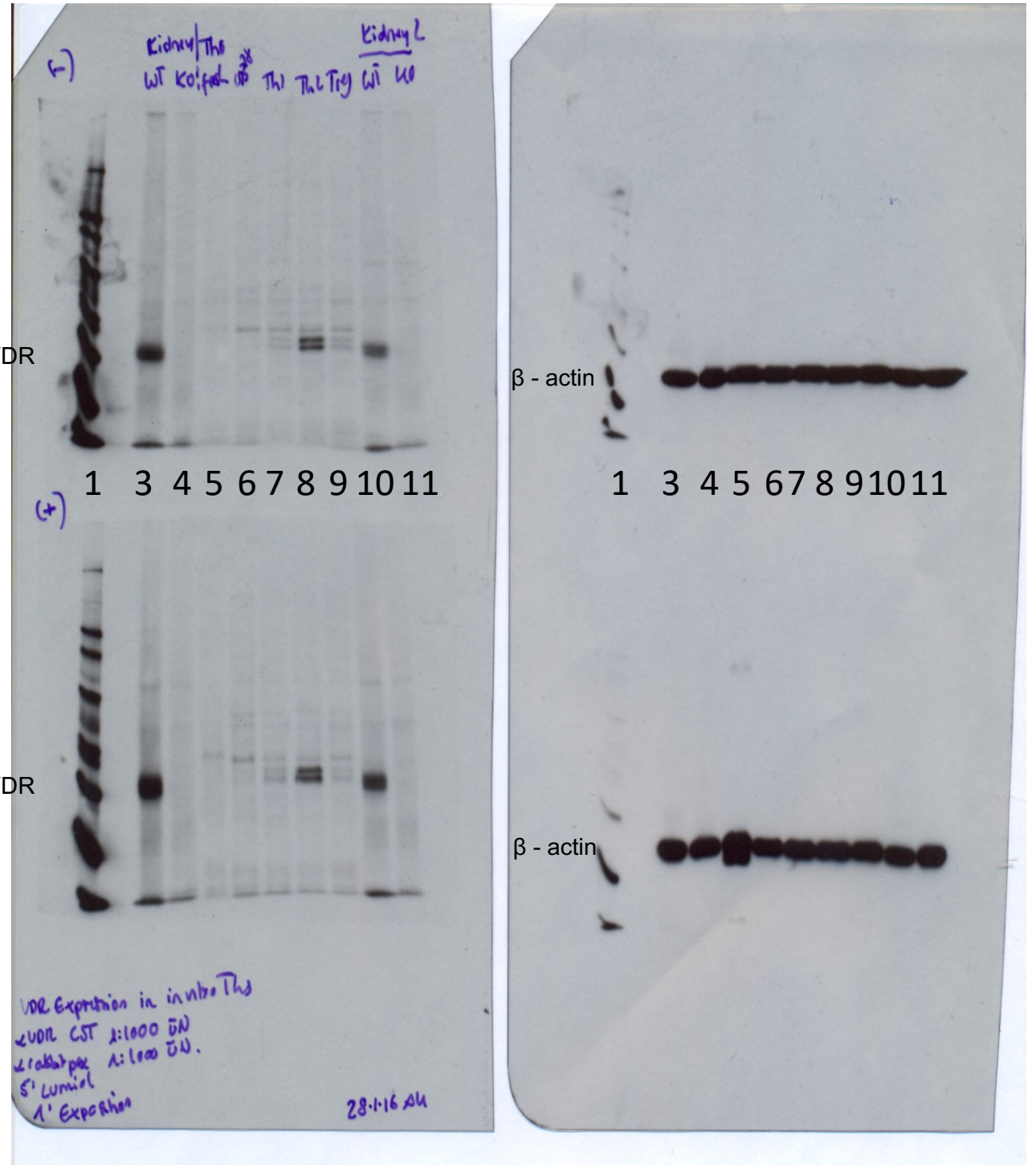

Loading order:
1- marker
2- empty
3- WT kidney sample: positive control
4- VDR-/- kidney sample: negative control
5- CD4+ CD62L+CD44- naïve T cells fresh
6- Th0 cells (24 h CD3 & CD28 stimulation)
7- in vitro Th1
8- in vitro Th2
9- in vitro iTreg
10- WT kidney sample: positive control
11- VDR-/- kidney sample: negative control

Supplementary Figure 1

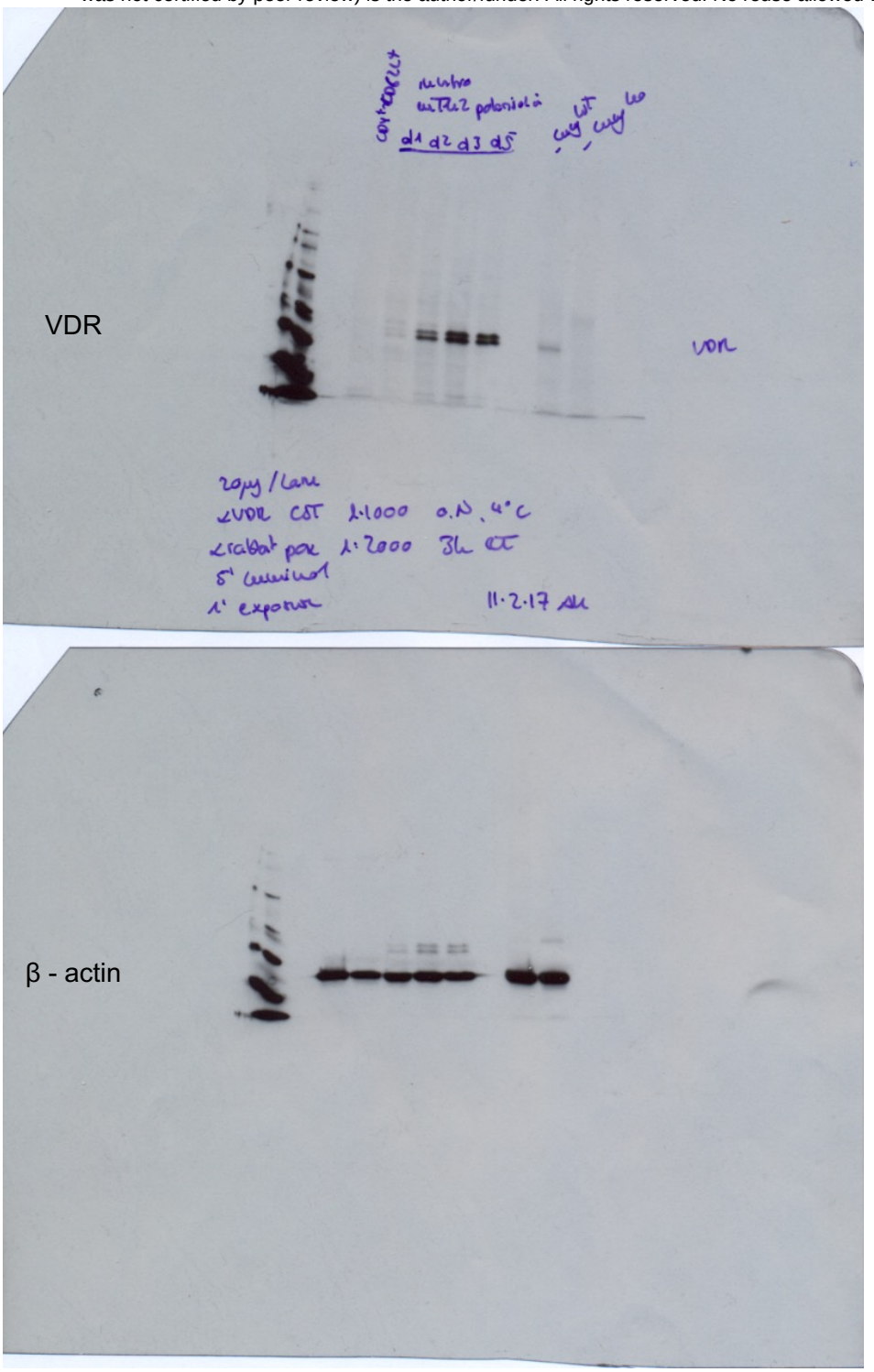

Loading order:
1- marker
2- empty
3- CD4+ CD62L+CD44- naïve T cells fresh
4- in vitro differentiating Th2 day 1
5- in vitro differentiating Th2 day 2
6- in vitro differentiating Th2 day 3
7- in vitro differentiating Th2 day 5
8- empty
9- WT lung sample: positive control
10- VDR-/- lung sample: negative control

Supplementary Figure 2